Journal of Medicinal Chemistry

Article

pubs.acs.org/jmc

Development of Novel Dual Binders as Potent, Selective, and Orally Bioavailable Tankyrase Inhibitors

Zihao Hua,*[,†] Howard Bregman,[†] John L. Buchanan,[†] Nagasree Chakka,[†] Angel Guzman-Perez,[†] Hakan Gunaydin,[∥] Xin Huang,[∥] Yan Gu,[∥] Virginia Berry,[‡] Jingzhou Liu,[‡] Yohannes Teffera,[‡] Liyue Huang,[‡] Bryan Egge,[⊥] Renee Emkey,[⊥] Erin L. Mullady,[⊥] Steve Schneider,[⊥] Paul S. Andrews,[⊥] Lisa Acquaviva,[§] Jennifer Dovey,[§] Ankita Mishra,[§] John Newcomb,[§] Douglas Saffran,[§] Randy Serafino,[§] Craig A. Strathdee,[§] Susan M. Turci,[§] Mary Stanton,[#] Cindy Wilson,[§] and Erin F. DiMauro*[,†]

[†]Department of Chemistry Research and Discovery, [‡]Department of Pharmacokinetics and Drug Metabolism, [§]Oncology Research, [∥]Department of Molecular Structure, [⊥]Bioassay and Profiling, and [#]Pharmaceutics, Amgen Inc., 360 Binney Street, Cambridge, Massachusetts 02142, United States

Supporting Information

ABSTRACT: Tankyrases (TNKS1 and TNKS2) are proteins in the poly ADP-ribose polymerase (PARP) family. They have been shown to directly bind to axin proteins, which negatively regulate the Wnt pathway by promoting β-catenin degradation. Inhibition of tankyrases may offer a novel approach to the treatment of *APC*-mutant colorectal cancer. Hit compound **8** was identified as an inhibitor of tankyrases through a combination of substructure searching of the Amgen compound collection based on a minimal binding pharmacophore hypothesis and high-throughput screening. Herein we report the structure- and property-based optimization of compound **8** leading to the identification of more potent and selective tankyrase inhibitors **22** and **49** with improved pharmacokinetic properties in rodents, which are well suited as tool compounds for further in vivo validation studies.

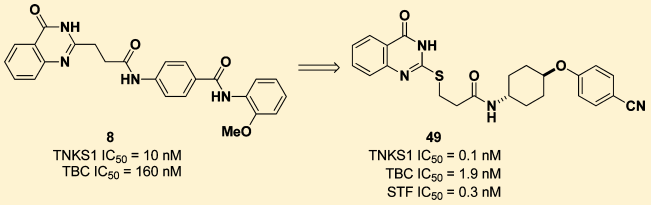

INTRODUCTION

The evolutionarily conserved Wnt/β-catenin (canonical) signaling transduction pathway plays a critical role in embryonic development and maintenance of homeostasis in mature tissues.[1] A key feature of the canonical pathway is the regulated proteolysis of the downstream effector β-catenin by the β-catenin destruction complex, which consists of adenomatous polyposis coli (APC), axis inhibition protein (axin), glycogen synthase kinase 3β (GSK3β), and casein kinase 1α (CK1α). The activity of the canonical pathway is dependent on the amount of β-catenin in the cytoplasm. In the absence of Wnt activation, the cytoplasmic β-catenin level is kept low through phosphorylation, mediated by the destruction complex, and subsequent ubiquitination and proteosomal degradation. Upon Wnt stimulation, the destruction complex dissociates, resulting in accumulation and translocation of active β-catenin to the nucleus and transcription of Wnt pathway responsive genes. Aberrant activation of the Wnt/β-catenin signaling pathway has been observed in many cancers.[2] Notably, most colorectal cancers (CRCs) are initiated by mutations of *APC*, leading to increased β-catenin mediated signaling.

Tankyrase 1 (TNKS1, PARP-5a) and tankyrase 2 (TNKS2, PARP-5b) are members of the poly ADP-ribose polymerase (PARP) family of 17 proteins that share a catalytic PARP domain. PARP proteins use nicotinamide adenine dinucleotide (NAD^+) as a substrate to transfer ADP-ribose polymers onto target proteins. This post-translational modification is termed PARsylation. PARP1 and PARP2, the two most characterized family members, have been pursued as cancer drug targets for more than a decade, although the specific cellular functions of many PARP proteins remain to be determined.[3] Tankyrases were first discovered as factors that regulate telomere homeostasis by modifying the negative regulator of telomere length, TRF1.[4] Recently, tankyrases have been shown to directly bind to and PARSylate axin proteins and have therefore gained increased attention as potential drug targets.[5] Axin, a negative regulator of the Wnt pathway, has been reported to be the concentration-limiting factor in regulating the efficiency of the β-catenin destruction complex. Overexpression of axin induces β-catenin degradation even in cell lines expressing truncated *APC*.[6] These findings suggest that a small molecule inhibitor of tankyrase activity would antagonize the Wnt/β-catenin signaling transduction pathway by stabilizing axin and promoting β-catenin degradation and might therefore be a useful therapeutic agent for suppressing the growth and survival of *APC* mutant CRC cells.

The first reports of potent and selective small molecule tankyrase inhibitors described two structurally distinct chemotypes, XAV939[7] and inhibitors of Wnt response (IWRs)[8]

Received: August 26, 2013
Published: December 2, 2013

   dx.doi.org/10.1021/jm401317z | *J. Med. Chem.* 2013, 56, 10003−10015

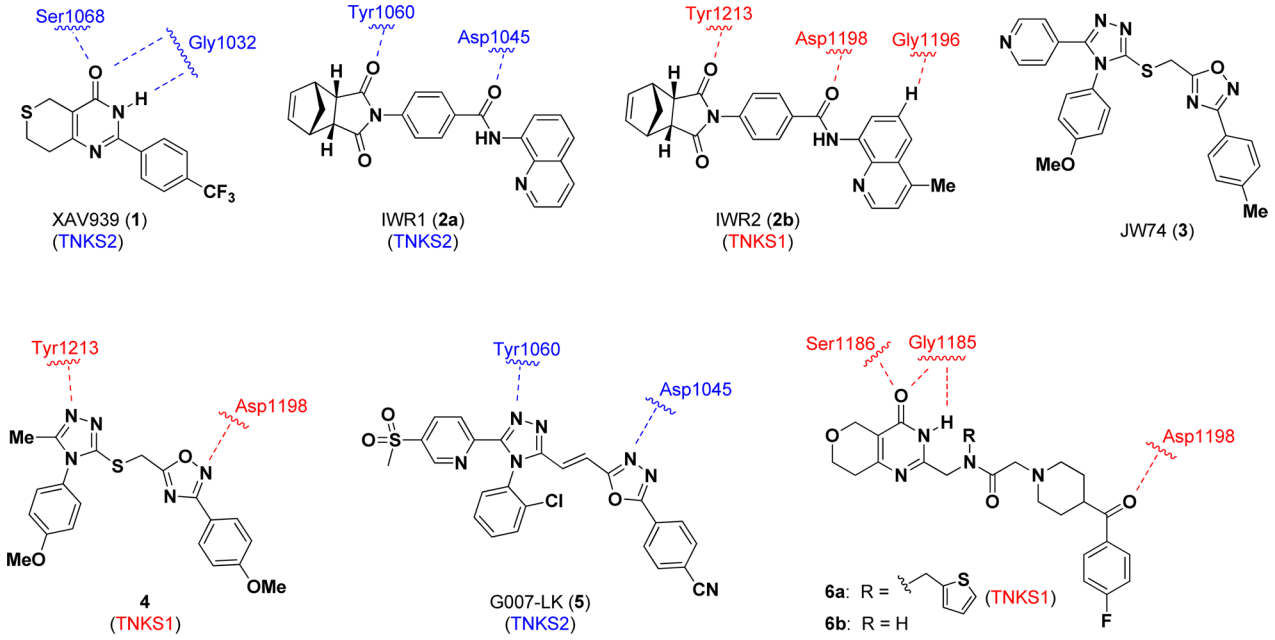

Figure 1. Structures of selected tankyrase inhibitors and their binding modes to TNKS1 or TNKS2 (indicated in parentheses).

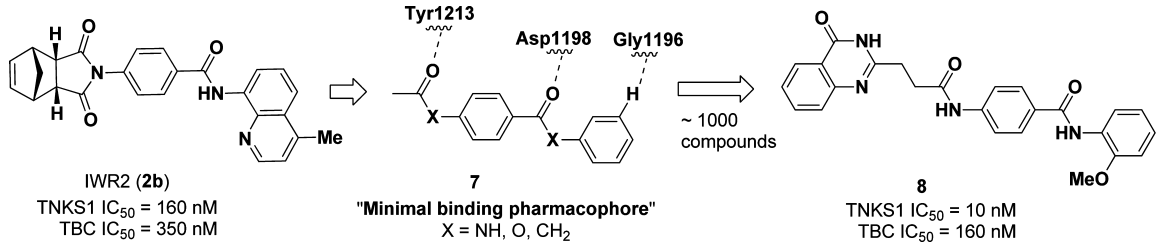

Figure 2. Identification of compound **8** as a tankyrase inhibitor via substructure search and screening.

(Figure 1). XAV939 was originally developed as a weak inhibitor of PARP1/2 (IC_{50} of 2.2 and 0.11 μM) but was demonstrated to be a more potent inhibitor of TNKS1 and TNKS2 with IC_{50} values of 11 and 4 nM, respectively. IWR2 inhibits TNKS1 and TNKS2 with IC_{50} values of 160 and 350 nM, respectively. The reported cocrystal structure of TNKS2 with XAV939 reveals ligand binding to the nicotinamide pocket through similar interactions as observed for other PARP1/2 inhibitor complexes, with three conserved hydrogen bonds between the ligand and the protein, via the carbonyl and NH group of the quinazolinone moiety.[9] A novel binding mode of IWR compounds to tankyrase was discovered both internally[10] and at Akademi University, Finland, by Lehtiö and coworkers[11] through high-resolution cocrystal structures of the human TNKS1 or TNKS2 catalytic domain in complex with IWR2 or IWR1. The TNKS1/IWR2 cocrystal structure reveals that IWR2 does not bind to the nicotinamide pocket but to an induced pocket that becomes available only upon binding of the IWR2 molecule. There are three hydrogen bonds between IWR2 and TNKS1: one between a carbonyl oxygen of the pyrrolidine dione group and the main chain NH of Tyr1213, another one between the carbonyl oxygen of the amide and the main chain NH of Asp1198, and one C−H···O═C hydrogen bond between the C−H at the 6-position of the quinoline and the main chain carbonyl oxygen of Gly1196. During the course of our investigations into the binding mode of IWRs, triazole compound JW74 (**3**) was reported as an inhibitor of Wnt signaling in a HEK293-STF assay.[12] More recently, two different analogues of JW74 (**4**[13] and G007-LK[14]) were independently disclosed as potent and selective inhibitors of TNKS1/2. The cocrystal structures of **4** and G007-LK complexed to TNKS1 or TNKS2 catalytic domains demonstrate ligand binding to the induced pocket similar to the IWR compounds, and also to a hydrophobic nook with the phenyl ring on triazole nitrogen. Further, a recent Genentech publication disclosed proof-of-concept antitumor efficacy with compound G007-LK in two *APC* mutant CRC models in mice.[15]

Toward identifying a potent and selective small molecule inhibitor of tankyrases,[16] we initiated a substructure search based on the novel binding motif derived from the IWR2/TNKS1 cocrystal structure. Approximately 1000 diverse compounds possessing the hypothetical minimal binding pharmacophore (**7**) were selected from the Amgen compound collection (Figure 2). High-throughput screening of these compounds with an enzymatic TNKS1 autoparsylation assay identified *N*-(2-methoxyphenyl)-4-(3-(4-oxo-3,4-dihydroquinazolin-2-yl)propanamido)benzamide (**8**) as the most potent inhibitor of tankyrase among them, with an IC_{50} value of 10 nM. Compound **8** also demonstrated potent cellular activity (IC_{50} = 160 nM) in a total β-catenin (TBC) degradation assay in SW480 cells.[17]

A cocrystal structure of compound **8** bound to TNKS1 revealed key interactions in both the induced pocket and the nicotinamide pocket. Structural comparison suggests that **8** overlays well with both XAV939 and IWR2. This "dual-

dx.doi.org/10.1021/jm401317z | J. Med. Chem. 2013, 56, 10003−10015

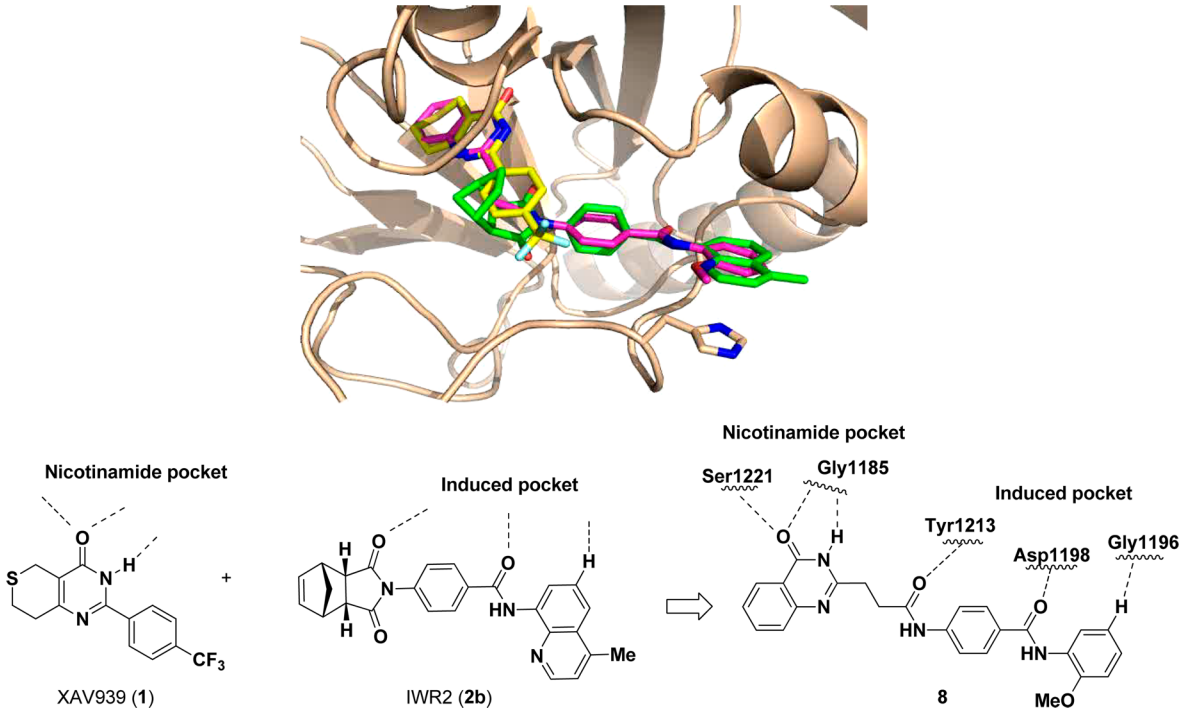

Figure 3. Overlay of cocrystal structures of XAV939 (PDB code 3UH4, yellow), IWR2 (PDB code 4DVI, green), and compound **8** (PDB code 4I9I, magenta) bound to TNKS1.

binding" mode, with the quinazolinone of **8** engaging the nicotinamide pocket and the rest of the molecule occupying the induced pocket (Figure 3), is presumably important for both affinity and specificity. The carbonyl oxygen of the quinazolinone is hydrogen-bonded to the side chain OH of Ser1221 and the main chain NH of Gly1185, while the NH of the quinazolinone is hydrogen-bonded to the main chain oxygen of Gly1185. The remainder of molecule **8** binds to the induced pocket that is accessed by the IWRs (**2a**, **2b**) and JW type (**3**–**5**) compounds, making an additional three hydrogen bonds to tankyrase: one between the left-hand-side amide oxygen and the main chain NH of Tyr1213, another one between the right-hand-side amide oxygen and the main chain NH of Asp1198, and a final one between the terminal phenyl group and the main chain oxygen of Gly1196 (C–H···O=C hydrogen bond). Both the methoxyphenyl group of **8** and the quinoline group of IWR2 engage in a π–π stacking interaction with the side chain of His1201 of the D-loop. We spectulated that this novel "dual-binding" tankyrase inhibitor chemotype that accesses both the nicotinamide pocket and the induced pocket may provide advantages in terms of potency and selectivity over similar members of the PARP family and other NAD^+-utilizing enzymes. Very recently, a tankyrase inhibitor (**6a**) that binds simultaneously to the nicotinamide pocket, induced pocket, and "nook" pocket has demonstrated in vivo acitivty as an antagonist of Wnt/β-catenin pathway activity. Interestingly, a truncated derivative **6b** that also binds to the nicotinamide pocket and the induced pocket demonstrated tankyrase inhibitory activity comparable to that of compound **8**.[16b]

Lead compound **8** suffered from poor plasma stability in mouse ($t_{1/2}$ = 40 min),[18] low solubility (6.6 μg/mL in fasted state simulated intestinal fluid (SIF) at pH 6.8), and high clearance (CL = 10.9 L h^{-1} kg^{-1}) in a rat iv pharmacokinetic (PK) study.[19] We initiated medicinal chemistry efforts toward the exploration of structure–activity relationships (SARs) within this new class of tankyrase dual binders, with the goals of improving the enzymatic and cellular potency and physicochemical and rodent PK properties in order to achieve adequate exposure for in vivo studies. During the course of these studies, we utilized rational structure- and property-based design.

CHEMISTRY

Our general strategy for the construction of the tankyrase inhibitors described herein involved amide coupling of carboxylic acid **21** with various *trans*-4-substituted cyclohexanamines. The synthesis of *trans*-4-(5-phenyloxadiazolyl)-cyclohexanamine **12** is shown in Scheme 1. A solution of *trans*-4-Boc-aminocyclohexanecarboxylic acid (**9**) was treated with benzhydrazide in the presence of DIPEA and HATU to

Scheme 1. Synthesis of *trans*-4-(5-Phenyl-1,3,4-oxadiazol-2-yl)cyclohexanamine (12)[a]

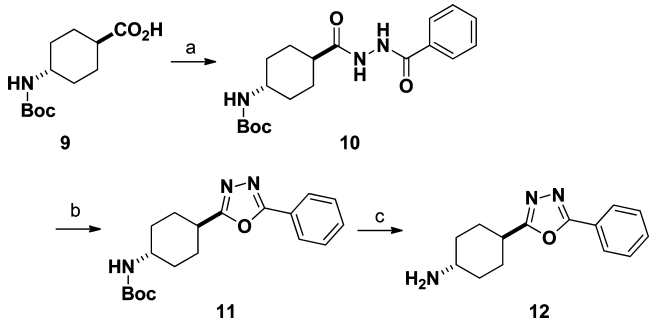

[a]Reagents and conditions: (a) benzhydrazide, DIPEA, HATU, CH_3CN; (b) TsCl, DIPEA; (c) TFA, CH_2Cl_2, 88% overall yield for three steps.

dx.doi.org/10.1021/jm401317z | J. Med. Chem. 2013, 56, 10003–10015

afford the corresponding diacylhydrazide **10**, which was subsequently treated with *p*-toluenesulfonyl chloride to afford the corresponding 1,3,4-oxadiazole **11**. Removal of the Boc-protecting group with trifluoroacetic acid afforded the desired *trans*-4-(5-phenyloxadiazolyl)cyclohexanamine **12**.

The synthesis of *trans*-4-phenoxycyclohexanamines is exemplified with *trans*-4-(4-fluorophenoxy)cyclohexanamine (**17**) and described in Scheme 2. Treatment of phthalimide (**13**) with ethyl chloroformate in the presence of triethylamine followed by displacement with *cis*-4-hydroxycyclohexanamine afforded the phthalimide-protected hydroxycyclohexanamine **15**. Mitsunobu reaction of **15** with 4-fluorophenol using DIAD and triphenylphosphine afforded the corresponding phenyl ether **16**. Subsequent removal of the phthalimide protecting group with hydrazine gave the desired *trans*-4-(4-fluorophenoxy)cyclohexanamine (**17**).

Scheme 2. Synthesis of *trans*-4-(4-Fluorophenoxy)cyclohexanamine (17)[a]

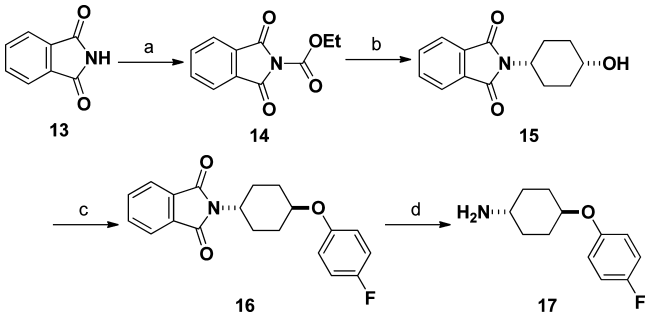

[a]Reagents and conditions: (a) ethyl chloroformate, Et_3N, DMF, 0 °C to room temperature, 50%; (b) *cis*-4-hydroxycyclohexamine·HCl salt, K_2CO_3, H_2O, 67%; (c) 4-fluorophenol, DIAD, PPh_3, THF, 51%; (d) NH_2NH_2, H_2O, EtOH, 95%.

The final assembly in the synthesis of tankyrase inhibitors is exemplified in Scheme 3 with *trans*-4-(5-phenyl-1,3,4-oxadiazol-2-yl)cyclohexanamine (**12**) as the right-hand-side motif. A mixture of 2-mercaptoquinazolinone (**18**) and *tert*-butyl 3-bromopropanoate (**19**) in acetone was refluxed in the presence of potassium carbonate to afford the desired quinazolinone **20**. Removal of the *tert*-butyl group with trifluoroacetic acid gave the corresponding carboxylic acid **21**. Treatment of carboxylic acid **21** with *trans*-4-(5-phenyl-1,3,4-oxadiazol-2-yl)-cyclohexanamine (**12**) in the presence of propylphosphonic acid anhydride (T3P) and triethylamine afforded the elaborated compound **22**.

Scheme 3. Synthesis of Dual Binder Analogues[a]

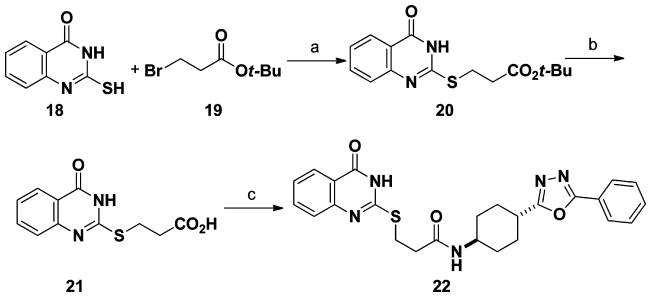

[a]Reagents and conditions: (a) K_2CO_3, acetone, 60 °C, 34%; (b) TFA, CH_2Cl_2, 95%; (c) *trans*-4-(5-phenyl-1,3,4-oxadiazol-2-yl)-cyclohexanamine (**12**), T3P, Et_3N, DMF, room temperature, 51%.

RESULTS AND DISCUSSION

Structure–Activity Relationship (SAR). Since a main goal of this program is to test the tankyrase mechanism in a mouse pharmacology model, we initially sought to improve the mouse plasma stability of our lead compound **8** (Table 1). A metabolite identification (MetID) study of **8** in fresh mouse plasma indicated that hydrolysis of the two amides contributed to the plasma instability, with the right-hand-side amide as the major hydrolytic liability. We first introduced a methyl group to the ortho position of each of the two aryl rings flanking the right-hand-side amide in an attempt to sterically block the amide hydrolysis. A methyl group at the ortho position of the terminal aryl ring (**23**) improved the plasma stability (increasing the half-life in mouse plasma by 8-fold), but the enzymatic potency on tankyrase decreased by 175-fold. A methyl group at the ortho position of the central aryl ring (**24**) led to a 21-fold decrease in tankyrase potency and comparable plasma instability to des-methyl lead **8**. Methylation of the

Table 1. SAR of the Right-Hand-Side Amide and Central Phenyl Ring toward Improving Mouse Plasma Stability

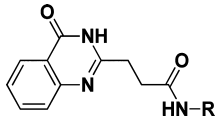

Compound	R	TNKS1[a] IC_{50} (μM)	SW480-TBC[b] IC_{50} (μM)	Mouse Plasma[c] $t_{1/2}$ (min)
8	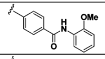	0.010	0.16	35
23		1.75	NA[d]	270
24	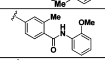	0.21	3.09	43
25	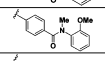	0.40	5.68	38
26	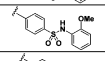	>46	NA	NA
27		0.40	Und[e]	>1000
28	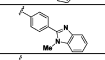	1.09	>10	>500
29	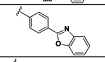	0.86	7.72	NA
30	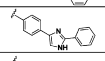	0.64	>10	53
31	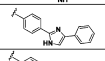	>46	NA	NA
32	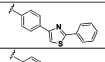	> 46	NA	NA
33	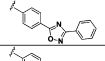	>46	NA	NA
34	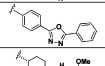	0.063	0.41	122
35	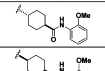	0.031	0.30	>1000
36	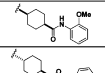	7.46	NA	>1000
37	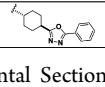	0.050	0.080	>500

[a,b]See Experimental Section for details of the assay. [c]See ref 18 for details of the mouse plasma stability assay. [d]NA = not measured. [e]Und = undefined (greater than 50% inhibition was achieved; however, curve fits could not be attained with acceptable confidence intervals).

dx.doi.org/10.1021/jm401317z | J. Med. Chem. 2013, 56, 10003–10015

right-hand-side amide nitrogen resulted in compound (**25**) with 40-fold loss of potency on tankyrase and no gain in plasma stability. Replacement of this right-hand-side amide with a sulfonamide (**26**) resulted in a dramatic loss of potency on tankyrase. We next examined a number of five-membered heteroaryl groups, directly fused to phenyl, as potential replacements of the right-hand-side amide functionality. Analogues with indazole (**27**), benzimidazole (**28**), and benzoxazole (**29**) offered excellent stability in mouse plasma but significantly decreased potency on tankyrase with IC_{50} values ranging from 0.40 to 1.09 μM. In order to maintain the excellent plasma stability demonstrated by these heteroarylamide replacements and improve the tankyrase activity, we explored analogues with a direct bond to the terminal phenyl group rather than a ring fusion to the phenyl group. Indeed, molecular modeling suggested that a terminal phenyl group bound directly to a five-membered heteroaryl ring might be appropriately positioned to engage in a $\pi-\pi$ stacking, hydrophobic interaction with the side chain of His1201 of the D-loop. Among the five-membered heteroaryls examined (imidazoles **30** and **31**, thiazole **32**, 1,2,4-oxadiazole **33**, and 1,3,4-oxadiazole **34**), only 1,3,4-oxadiazole **34** demonstrated good potency on tankyrase (IC_{50} = 63 nM) and showed improved stability in mouse plasma ($t_{1/2}$ = 122 min). The cocrystal structure of **34** bound to TNKS1 revealed a similar "dual-binding" mode as observed for compound **8** (Figure 4a). Structural comparison of **8**/TNKS1 and **34**/TNKS1 revealed that **34** and **8** overlay very well, with the quinazolinone of both **34** and **8** occupying the nicotinamide pocket and the rest of the molecules occupying the induced pocket. One of the nitrogen atoms from the oxadiazole of **34** forms a hydrogen bond to the main chain NH of Asp1198, similar to the right-hand-side amide oxygen of **8**. The terminal phenyl ring of **34** also engages in a $\pi-\pi$ stacking interaction with the side chain of His1201 of the D-loop, as hypothesized with modeling.

Moving next to address the mouse plasma instability by modulating the electronic property of the central phenyl group, we discovered that simple saturation of the central phenyl ring of compound **8** significantly improved the stability in mouse plasma (**35**, **36**). The resulting *trans*-cyclohexyl compound **35** showed only slightly decreased potency relative to lead compound **8** and 240-fold greater potency than the corresponding *cis*-cyclohexyl stereoisomer **36**. The combination of *trans*-cyclohexyl as the central ring and phenyl 1,3,4-oxadiazole as a right-hand-side amide surrogate resulted in compound **37**, which exhibited good enzymatic potency on tankyrase (IC_{50} = 50 nM) and significantly improved stability in mouse plasma ($t_{1/2}$ > 500 min) relative to **34**. Furthermore, it was devoid of the aniline toxicophore present in **35**. This compound also demonstrated good cellular potency, inhibiting total β-catenin levels in SW480 cells with an IC_{50} value of 80 nM.

With the good biological potency and plasma stability demonstrated by compound **37** having a *trans*-cyclohexyl group as the central ring and a phenyl-1,3,4-oxadiazole on the right-hand side, subsequent SAR studies were focused on modification of the left-hand-side quinazolinone moiety, which binds in the nicotinamide pocket and the ethylene linker between the quinazolinone (nicotinamide pocket binding motif) and the left-hand-side amide (induced pocket binding motif) (Table 2). Modification of this region was expected to improve the potency by aligning the left-hand side of the ligand to make improved binding contacts in and around the nicotinamide pocket. Replacing the phenyl group of the quinazolinone with a pyridine (**38**) resulted in a 15-fold loss of activity in both enzyme and cell assays. Saturation of the pyridine ring gave a compound (**39**) that is similarly active on tankyrase relative to **37** but much less potent in the cellular assay. Although the introduction of a polar piperidine (**40**) or pyrrolidine (**41**) ring to replace the linear ethylene linker showed slightly improved enzymatic activity and increased solubility relative to **37**, these analogues suffered a 5- to 10-fold decrease in cellular potency and rat liver microsomal (RLM) stability.[20] Further fine-tuning of the linear linker to better access both pockets was anticipated to afford increased biological activity. Replacing the benzylic carbon with a sulfur atom (**42**) showed 3-fold increased tankyrase activity and

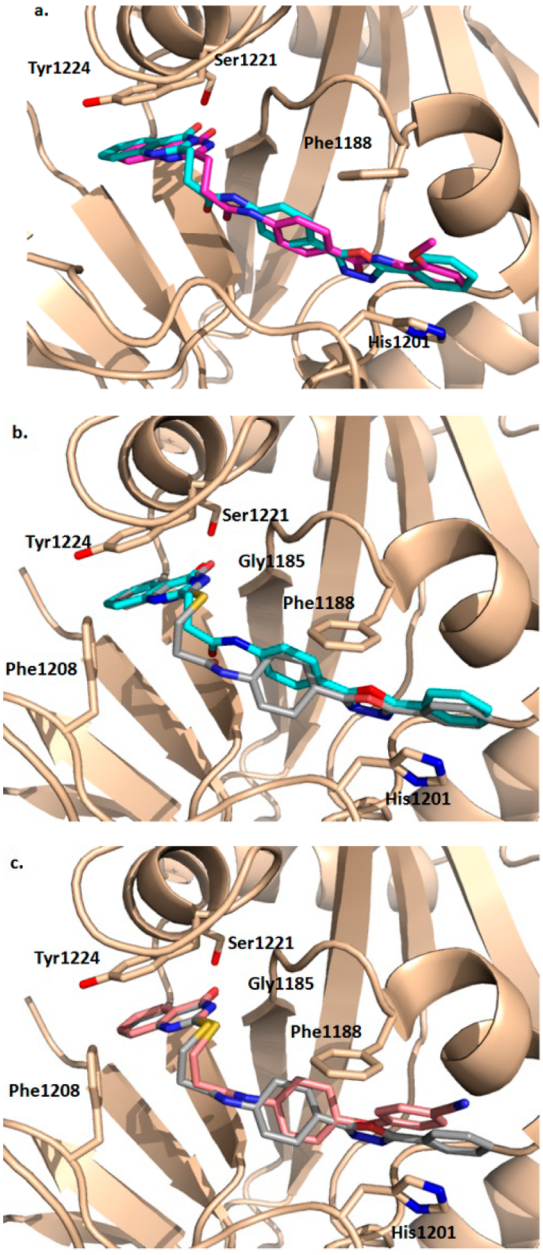

Figure 4. Overlays of cocrystal structures of TNKS1/TNKS inhibitor complexes: (a) structure overlay of **8** (magenta) and **34** (PDB code 4MSK, cyan); (b) structure overlay of **34** (cyan) and **22** (PDB code 4MSG, gray); (c) structure overlay of **22** (gray) and **49** (PDB code 4MT9, peach).

dx.doi.org/10.1021/jm401317z | *J. Med. Chem.* 2013, 56, 10003−10015

Table 2. SAR of the Nicotinamide Pocket Binding Motif and Linker

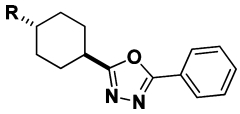

Compound	R	TNKS1 IC_{50} (μM)	SW480-TBC IC_{50} (μM)	RLM CL_{int} [b] (μl/min/mg)	SIF (μg/mL)
37	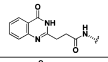	0.050	0.080	< 14	16.2
38		0.80	1.95	24	NA[a]
39		0.037	1.02	< 14	NA
40	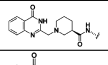	0.027	1.17	206	43.0
41	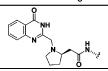	0.021	0.50	> 399	42.0
42		0.016	0.091	20	1.0
43	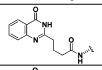	0.002	0.017	20	11.0
22	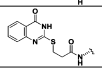	0.0001	0.004	57	7.0
44	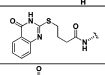	0.001	0.10	159	1.0
45	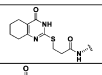	0.0002	0.011	60	8.0
46		0.031	2.13	< 14	53.0

[a]NA = not measured. [b]Rat liver microsomal intrinsic clearance.[21] CL_{int} in microsomal stability was measured using the substrate depletion method. Metabolism was initiated by addition of test compounds to the prewarmed (37 °C) incubation mixture (0.25 mg of microsomal protein/mL, 1 mM NADPH, 2 mM magnesium chloride in 50 mM potassium phosphate buffer, pH 7.4) to achieve a final concentration of 1 μM. Disappearance of parent was determined after 30 min of incubation at 37 °C.

similar potency in the cellular assay relative to **37**. Homologation of the linker by one methylene resulted in compound **43** showing a 8-fold increase of tankyrase activity relative to **42** and an IC_{50} of 17 nM in the cellular assay. Further elongation of the linker by replacing the benzylic carbon with a sulfur atom gave compound **22**, with excellent potency in both tankyrase (IC_{50} = 0.1 nM) and cellular (TBC IC_{50} = 4 nM) assays. Further homologation of the linker resulted in compound **44**, which exhibited significantly decreased potency in enzyme and cell, lower solubility, and reduced microsomal stability. Partial saturation of the quinazolinone of **22** afforded compound **45** with similar enzymatic potency, aqueous solubility, and microsomal stability but slightly decreased cellular potency relative to **22**. Removal of the quinazolinone phenyl ring resulted in compound **46**, leading to a substantial loss in tankyrase activity and cellular potency.

The cocrystal structure of **22** and TNKS1 revealed binding to both the nicotinamide pocket and the induced pocket, similar to **34** (Figure 4b). The central cyclohexyl ring of **22** and the central phenyl ring of **34** occupy the same spatial pocket but are oriented almost perpendicular to each other. More importantly, the sulfur ethylene linker of **22** is engaging in additional hydrophobic interactions with the side chain of Phe1208 of the D-loop, consistent with the observed increase in potency. The conformation of the sulfur ethylene linker on **22** is quite different from the close structural analogue **43** (three-carbon linker). The C−S−C bond angle in **22** is 104° while the C−C−C bond angle in **43** is 116°, which allows better hydrophobic interaction for **22** with the side chain of Phe1208 of the D-loop. In addition, the sulfur atom of **22** engages in a favorable S···O=C interaction[22] with the backbone carbonyl of Gly1185 and positions the amide carbonyl and the oxadiazole groups of **22** for engaging in more favorable H-bonding interactions with the backbone NHs of Tyr1213 and Asp1198, respectively. These two distances are approximately 2.8 and 2.9 Å for **22** and 2.9 and 3.1 Å for **43**. Furthermore, a dihedral scan calculation suggested that the three-atom linker with sulfur at the benzylic position has a strong preference for planar geometry and **22** binds with a geometry (6° away from planarity) that is very close to the preferred geometry.[23]

Although compound **22** demonstrated excellent enzymatic and cellular potency, we sought to develop a compound with similar biochemical potency and improved physicochemical and pharmacokinetic properties in rodents for extensive in vivo studies. Toward this end, we focused on replacing the right-hand-side phenyl-1,3,4-oxadiazole moiety with a smaller group that maintained the key hydrogen bonding and hydrophobic interactions with the induced pocket. Molecular modeling suggested that a simple phenoxy group might be sufficient to replace the phenyl-1,3,4-oxadiazole moiety with maintenance of the π−π stacking interaction with the side chain of His1201 of the D-loop. Thus, a diverse series of phenoxy and pyridinyloxy compounds were prepared and tested in both enzymatic and cellular assays (Table 3). Not surprisingly, all the phenoxy and

Table 3. SAR of Right-Hand-Side Phenoxy Group To Replace the Phenyl-1,3,4-oxadiazole

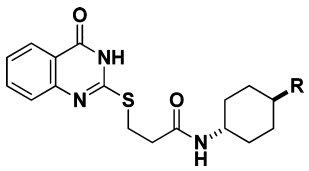

Compound	R	TNKS1 IC_{50} (nM)	SW480-TBC IC_{50} (nM)
8	--	10	160
22		0.1	3.7
47		0.2	16.7
48		0.1	20.0
49		0.1	1.9
50		0.2	6.9
51		0.2	15.4
52		0.2	120.0
53		0.2	47.8
54		0.3	24.2
55		0.2	8.1

pyridinyloxy compounds showed excellent inhibitory potency on tankyrase, similar to **22**. Unfortunately, most of the phenoxy compounds suffered from a 4- to 30-fold loss in cellular potency relative to **22**, with the exceptions of **49**, **50**, and **55**, which emerged as new leads.

To understand the structural basis for the excellent enzymatic potency observed with these phenoxy compounds, a cocrystal structure of compound **49** with TNKS1 was

dx.doi.org/10.1021/jm401317z | J. Med. Chem. 2013, 56, 10003−10015

obtained and compared with the cocrystal structure of **22** with TNKS1. As shown in Figure 4c, the quinazolinone ring of **49** binds in the nicotinamide pocket and overlays very well with the quinazolinone ring of **22**. The phenoxy oxygen of **49** forms a hydrogen bond with Asp1198, similar to the hydrogen bond formed by one of the nitrogen atoms from the oxadiazole of **22**. The terminal phenyl ring of **49** also engages in a $\pi-\pi$ stacking interaction with the side chain of His1201 of the D-loop.

To identify a compound for in vivo studies in rodents, selected phenyloxadiazole compounds (**22**, **45**) and phenoxy compounds (**49**, **50**, and **55**) were further characterized with enzymatic TNKS2 autoparsylation assay and additional functional cellular assays: axin2 accumulation in SW480 cells, to evaluate the compound's ability to cause stabilization and accumulation of axin protein levels, and Super-Topflash (STF) reporter transcription in DLD-1 cells, a second colorectal cancer cell line with truncated *APC*, to evaluate the compound's downstream inhibitory activity on Wnt-associated gene transcription (Table 4). All of the selected compounds showed

Table 4. Profile of Selected Compounds in Additional Functional Cellular Assays

compd	TNKS1 IC_{50} (nM)	TNKS2 IC_{50} (nM)	SW480-TBC IC_{50} (nM)	SW480-axin2 EC_{50} (nM)	DLD1-STF IC_{50} (nM)
34	63	13	410	2450	NA[a]
37	50	14	80	640	NA[a]
22	0.1	4.1	3.7	3.9	0.6
45	0.2	2.5	11	14	1.3
49	0.1	7.6	1.9	4.0	0.3
50	0.2	6.2	6.9	6.8	0.7
55	0.2	0.4	8.1	8.4	1.1

[a]NA = not measured.

good potency in the TNKS2 enzymatic assay, which is desirable because of possible redundancy between these isoforms. Early lead compounds (**34** and **37**) with a two-carbon linker, being less potent in the enzyme assay, consistently displayed only modest potency in all the cellular assays. Lead-optimized phenyloxadiazole compounds (**22** and **45**) and phenoxy compounds (**49**, **50**, and **55**) having good enzymatic potency and cellular potency in the SW480-TBC cellular assay demonstrated excellent potencies in TNKS2 autoparsylation assay and the two additional functional cellular assays.

Pharmacokinetic Profile. Having identified leads showing excellent in vitro tankyrase cellular inhibitory activity, we carried out in vivo PK evaluations of phenyloxadiazole compounds (**22** and **45**) and phenoxy compounds (**49**, **50**, and **55**). The PK data for intravenous (iv) dosing in rat (0.5 mg/kg) and oral (po) dosing in mouse (30 mg/kg) are shown in Table 5. Phenyloxadiazole compound **22** and phenoxy compounds **49** and **50** all displayed low to moderate clearance, small volume of distributions, and short (**50**) to moderate (**22**, **49**) half-lives in rats.[24] Upon oral administration of a single dose of 30 mg/kg to mice, phenyloxadiazole compound **22** exhibited significantly higher oral total and free exposure than the close structural analogue **45**. Among the three phenoxy compounds, **49** showed higher oral free exposure in mice than **50** and **55**. In light of their good oral exposure and excellent cellular activity, we decided to progress phenyloxadiazole compound **22** and phenoxy compound **49** to further in vitro selectivity profiling and in vivo pharmacodynamic profiling in tumor-bearing mice.

Selectivity Profile. Prior to in vivo testing, compounds **22** and **49** were screened for inhibitory activity against PARP1/2 and an extensive panel of kinases. Both compounds showed excellent selectivity (>10 000-fold) over PARP1/2.[26] Compounds **22** and **49** showed less than 50% inhibition when tested at 1.0 μM across a panel of 100 kinases which were chosen to cover the diversity of the kinome.[27]

Pharmacodynamic Profile. Both **22** and **49** were evaluated for Wnt-pathway specific pharmacological activity in mouse tumor pharmacodynamic (PD) models. Upon once daily oral administration (at 10 and 50 mg/kg) to mice (n = 4) bearing human DLD-1 tumors for 3 days, both compounds exhibited statistically significant, dose-dependent axin2 accumulation (2.1- to 3.5-fold) and inhibition of STF (51−79%) at day 3 (24 h after the last dose) (Figures 5 and 6). Terminal

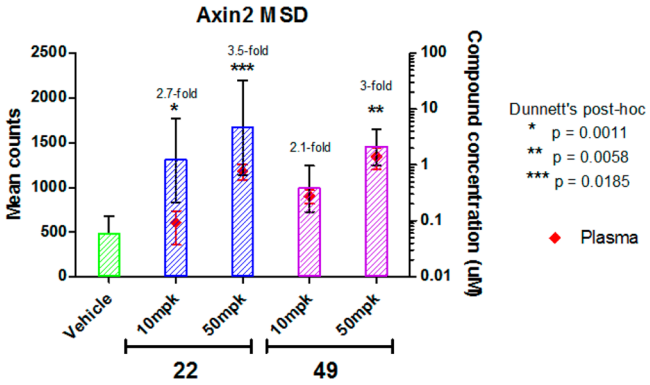

Figure 5. Compounds **22** and **49** stabilize axin2 in a DLD-1 mouse tumor PD model (3 days of q.d. dosing at 10 and 50 mg/kg).

Table 5. Mean PK Parameters after Intravenous Dose (iv) in Rat[a] or Oral Dose (po) in Mouse[b]

	rat iv (0.5 mg/kg)			mouse po (30 mg/kg)			
compd	CL (L h^{-1} kg^{-1})	V_{ss} (L kg^{-1})	$t_{1/2}$ (h)	$AUC_{0-\infty}$ (μM h)	C_{max} (μM)	t_{max} (h)	mouse f_u[d]
22	0.83	0.70	1.8	49.5	18.7	0.58	0.017
45	NA[c]	NA[c]	NA[c]	5.3	3.6	3.23	0.012
49	0.12	0.32	2.8	141.0	24.2	1.50	0.006
50	0.66	0.40	0.7	11.5	7.0	0.67	0.032
55	NA[c]	NA[c]	NA[c]	100.0	15.1	1.58	0.002

[a]Male rat. [b]Male CD-1 mice; 10% Pluronic F68, 30% HPBCD, 60% water; pH adjusted to 10.0 with sodium hydroxide for **22**, **45**, **49**, and **50**, pH adjusted to 2.5 with methanesulfonic acid for **55**. [c]NA = not measured. [d]Fraction unbound in mouse plasma was determined in duplicate by equilibrium dialysis using the rapid equilibrium dialysis device. Plasma was spiked with test compounds at a final concentration of 5 μM and dialyzed against plasma water (ultrafiltrate) for 5 h in a CO_2 incubator at 37 °C.[25]

dx.doi.org/10.1021/jm401317z | J. Med. Chem. 2013, 56, 10003−10015

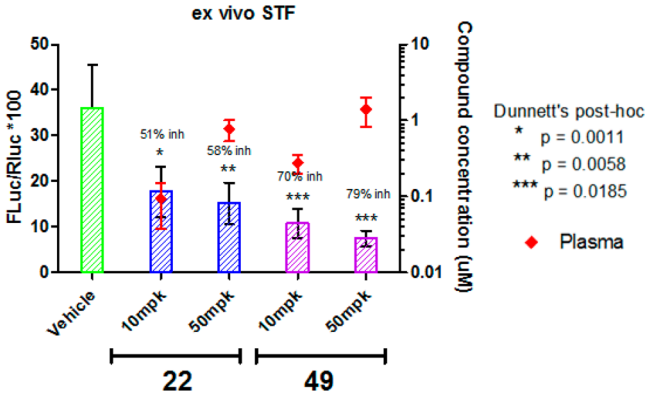

Figure 6. Compounds **22** and **49** inhibit STF in a DLD-1 mouse tumor PD model (3 days of q.d. dosing at 10 and 50 mg/kg).

plasma samples (24 h after last dose) were collected to estimate compound exposure. For the 50 mg/kg dose group, mean unbound plasma concentrations were 13 and 9 nM for **22** and **49**, respectively. These concentrations are 2- to 3-fold over the respective in vitro axin2 EC_{50} values (4 nM for both compounds) and 22- and 30-fold over the respective STF inhibition IC_{50} values (0.6 nM for **22**, 0.3 nM for **49**).

SUMMARY AND CONCLUSION

Substructure searching of the Amgen collection, based on a minimal binding pharmacophore hypothesis, resulted in the identification of hit compound **8**, which was determined by X-ray crystallography to interact with tankyrase in a novel "dual-binding" fashion, occupying both the nicotinamide pocket (similar to XAV939) and the induced pocket (similar to IWRs and JWs). Our investigation of SAR made use of both structure-based and physicochemical-property-based optimization, with guiding data from X-ray crystallography and pharmacokinetic analysis. These efforts led to the identification of oxadiazole **22** and phenyloxy **49**, which showed excellent in vitro potency as measured by the inhibition of tankyrase 1 and 2, total β-catenin reduction or degradation, STF gene transcription, and axin accumulation in SW480 and DLD-1 cells. Furthermore, leads **22** and **49** demonstrated oral activity in a mouse DLD-1 tumor PD model of axin accumulation and ex vivo STF inhibition.

The leads presented herein are expected to be of considerable utility in future studies aimed at elucidating the potential of selective pharmacological tankyrase inhibition in cancer therapy. Specifically, several analogues from this novel dual-binder class are extremely potent and selective and therefore anticipated to be of value in the search for antiproliferative activity in various cancer cell lines. Orally bioavailable leads **22** and **49** are particularly suited for the exploration of extended dosing studies in rodents, for understanding the suppression of growth and survival of tumors and overall toxicological profiles.

EXPERIMENTAL SECTION

Tankyrase 1 and 2 Assays. The tankyrase 1 biochemical activity of the compounds was assayed in the following assay buffer (50 mM MOPS, pH 7.5, 100 mM NaCl, 2.5 mM $MgCl_2$, 0.01% Tween-20, 0.05% BSA, and 1 mM DTT) as follows: 0.25 nM of 6× HIS-tankyrase 1 (no. 1091-1325) was incubated in the presence of compound (DMSO 1.85% final) in a Perkin-Elmer 384-well Proxiplate Plus (catalog no. 6008289) with 400 nM NAD for 60 min at ambient temperature. The assay was then stopped with the above assay buffer containing a 0.6 μM inhibitor and the following detection components: 0.05 μg/mL monoclonal anti-PAR antibody (Trevigen catalog no. 4335-MC-01K-AC) prebound for 60 min with 0.63 μg/mL protein G AlphaLisa acceptor bead (Perkin-Elmer catalog no. AL102M) and 5 μg/mL AlphaLisa nickel chelate donor bead (Perkin-Elmer catalog no. AS101M). The sample was incubated for 16 h at room temperature in the dark, and results were read on a Perkin-Elmer Envision multilabel reader using the default program set with laser excitation at 680 nm and emission at 615 nm. Assay standards were the following: 66 runs with standard which yielded a mean of 0.0086 μM with a standard deviation of 0.00038; 42 runs with a different standard which yielded a mean of 0.0013 μM with a standard deviation of 0.000 64.

Total β-Catenin (TBC) Assay. TNKS inhibition results in degradation of the total pool of β-catenin in SW-480 cells colorectal cells. SW480 cells do not express E-cadherin and thus do not have membrane associated ("non-signaling") β-catenin which interferes with Wnt pathway activity analysis. Cells were seeded at 10 000/well in CellBIND 96-well in 60 μL of normal growth medium (MEMα supplemented with 10% heat inactivated FBS, GlutaMAX, pyruvate, and 10 mM HEPES). A 10-point, 3-fold dilution series for each TNKS inhibitor was constructed, and 20 μL of each diluted compound was transferred to the plated SW-480 cells (resulting in a final vehicle (DMSO) concentration of 0.1%). The plates were incubated at 37 °C for 40−48 h, after which the medium was removed and the cells were lysed with 75 μL/well MSD lysis buffer. A goat anti-rabbit MSD plate (catalog no. L41RA-1) was coated with 25 μL of 5 μg/mL of Cell Signaling antitotal β-catenin polyclonal (catalog no. 9562, lyophilized, carrier-free special order) and incubated overnight in a cold room with gentle shaking. The plate was then blocked with 150 μL of blocker "A" per well and washed 4 times with 150 μL/well TBS-T wash buffer (150 mM NaCl, 50 mM Tris, pH 7.5, 0.02% Tween-20). Cell lysates (75 μL) were transferred to prepared MSD plates and incubated at 4 °C overnight with gentle shaking. The next day MSD plates were washed with TBS-T wash buffer and the antitotal β-catenin mAb (catalog no. 610153) detection antibody conjugated to SULFO-TAG was added. The detection antibody was incubated for 1 h at room temperature with vigorous shaking, after which plates were washed and processed for analysis by the addition of 150 μL/well MSD read 4× buffer T with surfactant. The plates were read, and the data were captured on the SECTOR imager 6000. Assay standards were the following: 54 runs with a standard which yielded a mean of 0.157 μM with a standard deviation of 0.116; 38 runs with another standard which yielded a mean of 0.063 μM with a standard deviation of 0.041.

Axin2 Accumulation Assay. TNKS inhibition results in axin2 accumulation into distinct cytoplasmic foci which were visualized and quantified using a high-content imaging system (Cellomics ArrayScan). SW480 cells were grown under normal culture conditions (RPMI 1640, 10% HI FBS, and 1× sodium pyruvate). On the day of the assay, cells were plated at 2500 cells per well in 60 μL of assay medium in Perkin-Elmer Black 384 ViewPlates (Fisher, no. 509052489). TNKS compounds were diluted to generate a 22-point dose titration in medium and incubated with the cells for 24 h at 37 °C, 5% CO_2. The next day the cells were fixed for 15 min in 4% paraformaldehyde and 0.1% Triton, washed in PBS, and blocked in PBS with 0.1% Tween-20 and 1% normal goat serum. The cells were stained with an axin2 primary antibody (Sigma, no. SAB1100677-200UL) at 1:10000 overnight at 4 °C and an Alexa 488-labeled secondary antibody (Invitrogen, A11008). The nuclei were visualized with Hoechst dye. The axin2 foci were quantified on the Cellomics ArrayScan (a variation of the compartmental analysis protocol was optimized, and data were analyzed using MEAN_RingSpotAvgIntenCh2), and EC_{50} values were calculated. Assay standards were the following: 18 runs with a standard which yielded a mean of 0.311 μM with a standard deviation of 0.173. Eighteen runs with another standard which yielded a mean of 0.114 μM with a standard deviation of 0.065.

DLD-1 STF Assay. *Constitutively Activated Wnt Pathway Reporter Assay (APC Mutant Cancer Cell Context).* DLD-1 colorectal cells

engineered with an 8× TCF promoter-driven firefly (FF) luciferase gene (Wnt reporter) along with an EF1a promoter-driven *Renilla* (RN) luciferase gene (control reporter) were used to measure the potency of tankyrase compounds in the context of the constitutively activated Wnt pathway due to mutated *APC* in colorectal cancer cells. The engineered DLD-1 cells were plated at a density of 10 000 cells/well in black, clear-bottom, 96-well View plates (PerkinElmer) in normal growth medium (RPMI with 10% FBS with no antibiotics). Tankyrase inhibitors were transferred to cells from a 3-fold serially diluted compound plate. A 10-point dilution series was tested starting at 10 μM. The plates were incubated at 37 °C for 40−48 h. The Dual-Glo reagents (Promega) were added as directed by the manufacturer to assess the firefly (FF) and *Renilla* (RN) luciferase activity. Luciferase activity was measured using the EnVision multilabel plate reader (PerkinElmer).

DLD-1 Tumor PD in Mouse. Subcutaneous tumors were formed in athymic nude mice using DLD-1 human colon cancer cell line that had been engineered to express firefly luciferase under a Wnt-responsive SuperTopFlash (STF) promoter and *Renilla* luciferase under a constitutive promoter. Once tumors reached approximately 250 mm^3, tumor bearing animals were randomized into groups of 4 and then animals were dosed for 3 days with either compound or vehicle orally q.d. Tumors for protein analysis and plasma for PK were collected 14 h after the last dose. Quantitation of axin2 protein was done using an MSD assay (MesoScale Discovery) using an axin2 antibody from Genetex for capture and a sulfotagged antibody from R&D Systems for detection. STF transcription assay was done using the Dual-Glo luciferase assay from Promega, and firefly luciferase values were normalized using the *Renilla* luciferase values.

Chemistry. General. Unless otherwise noted, all materials were obtained from commercial suppliers and used without further purification. Anhydrous solvents were obtained from Aldrich and used directly. All reactions involving air- or moisture-sensitive reagents were performed under a nitrogen or argon atmosphere. Purity (3 min methods only) and reaction analyses were measured using Agilent 1100 series high performance liquid chromatography (HPLC) systems with UV detection at 254 and 215 nm (system A consisting of Agilent Zorbax SB-C18 3.0 mm × 50 mm, 3.5 μm, 5−95% CH_3CN in H_2O with 0.1% TFA for 3.6 min at 1.5 mL/min or Halo Phenyl-Hexyl, 3 mm × 50 mm, 2.7 μm, 5−95% CH_3CN in H_2O with 0.1% TFA for 1.01 min at 2.0 mL/min; system B consisting of Waters Xbridge C18, 3 mm × 50 mm, 3.5 μm, 5−95% CH_3CN in H_2O with 0.1% formic acid for 3.6 min at 1.5 mL/min). Silica gel chromatography was generally performed with prepacked silica gel cartridges (Biotage, Teledyne-Isco or Interchim). Library purification methods were as follows: preparative LC/MS, Waters autopurification system; liquid transfer system, Tecan; drying system, Genevac; preparative column, Xbridge (19 mm × 100 mm, C18, 10 μm); flow rate, 40 mL/min; general gradient, 5−95% B, 0.1% additive in both A and B; 10 min gradient; mobile phase A, water; mobile phase B, acetonitrile; additive, TFA or NH_4OH. ^1H NMR spectra were recorded on a Bruker AV-400 (400 MHz) spectrometer or a Varian 400 MHz spectrometer at ambient temperature. All observed protons are reported as parts per million (ppm) downfield from tetramethylsilane (TMS) or other internal reference in the appropriate solvent indicated. Data are reported as follows: chemical shift, multiplicity (s = singlet, d = doublet, t = triplet, q = quartet, br = broad, m = multiplet), coupling constants, and number of protons. Low-resolution mass spectrometry (MS) data were determined on an Agilent 1100 series LCMS with UV detection at 254 and 215 nm and a low resonance electrospray mode (ESI). All the compounds were determined to be ≥95% purity by HPLC.

***trans*-4-(5-Phenyl-1,3,4-oxadiazol-2-yl)cyclohexanamine (12).** To a mixture of *trans*-4-((*tert*-butoxycarbonyl)amino)-cyclohexanecarboxylic acid (0.52 g, 2.12 mmol) and benzhydrazide (0.29 g, 2.1 mmol) in acetonitrile (10 mL) at room temperature was added *N*,*N*-diisopropylethylamine (1.1 mL, 6.4 mmol), followed by HATU (0.89 g, 2.3 mmol). The resulting mixture was stirred at room temperature for 19 h. Then extra *N*,*N*-diisopropylethylamine (0.4 mL) was added followed by *p*-toluenesulfonyl chloride (1.21 g, 6.4 mmol), and the mixture was stirred at room temperature for 24 h. The reaction mixture was then poured into 14% aqueous NH_3 (20 mL), stirred for 15 min, then transferred to a separatory funnel and diluted with DCM and water. The organic layer was separated, and the aqueous layer was extracted with DCM. The combined organic layers were washed with brine, dried over anhydrous sodium sulfate, filtered, and concentrated. The crude reaction mixture was purified (ISCO 12 g column, 0−85% EtOAc−heptanes). The product-containing fractions were concentrated and loaded onto a 70 mL SCX-2 column with MeOH−DCM and eluted with 2.0 M NH_3 in MeOH. The crude *tert*-butyl (*trans*-4-(5-phenyl-1,3,4-oxadiazol-2-yl)cyclohexyl)carbamate (**11**) was taken directly onto the next step without further purification.

To a solution of crude *tert*-butyl *trans*-4-(5-phenyl-1,3,4-oxadiazol-2-yl)cyclohexylcarbamate (**11**) in DCM (10 mL) at room temperature was added trifluoroacetic acid (0.98 mL, 12.7 mmol). The resulting mixture was stirred at room temperature for 19 h. The mixture was concentrated and loaded onto a 70 mL SCX-2 column with MeOH−DCM and eluted with 2.0 M NH_3 in MeOH to afford *trans*-4-(5-phenyl-1,3,4-oxadiazol-2-yl)cyclohexanamine (0.45 g, 88%). ^1H NMR (400 MHz, DMSO-d_6) δ 7.95−8.05 (m, 2 H), 7.53−7.68 (m, 5 H), 2.94−3.15 (m, 2 H), 2.15−2.29 (m, 2 H), 2.02−2.10 (m, 2 H), 1.67 (dq, J = 3.2, 12.9 Hz, 2 H), 1.47 (dq, J = 3.3, 12.5 Hz, 2 H); m/z (ESI) 244.2 $(M + H)^+$.

Ethyl 1,3-Dioxoisoindoline-2-carboxylate (14). To a solution of phthalimide (2.00 g, 13.6 mmol) and triethylamine (2.75 g, 27.2 mmol) in DMF (10 mL) at 0 °C was added ethyl chloroformate (1.30 mL, 13.6 mmol) dropwise over a period of 0.5 h. The reaction mixture was allowed to warm to ambient temperature and further stirred for 2 h. After completion of the reaction, the reaction mixture was treated with ice−water, resulting in precipitation of a white solid. The precipitate was filtered and washed with cold water to obtain crude ethyl 1,3-dioxoisoindoline-2-carboxylate (1.50 g, 50%) as a white solid. ^1H NMR (400 MHz, $CDCl_3$) δ 7.86−7.99 (m, 4 H), 4.53 (q, J = 7.2 Hz, 2 H), 1.45 (t, J = 7.2 Hz, 3 H).

2-(*trans*-4-(4-Fluorophenoxy)cyclohexyl)isoindoline-1,3-dione (16). To a solution of crude ethyl 1,3-dioxoisoindoline-2-carboxylate (0.40 g, 1.8 mmol) and *cis*-4-aminocyclohexanol hydrochloride (0.28 g, 1.8 mmol) in water (4 mL) at 0 °C was added potassium carbonate (0.76 g, 5.5 mmol) portionwise. After 0.5 h, the reaction mixture was allowed to warm to ambient temperature and stirred further for 1 h. The resulting precipitate was filtered and dried in air to obtain crude 2-(*cis*-4-hydroxycyclohexyl)isoindoline-1,3-dione (**15**) (0.30 g, 67%) as a white solid.

To a mixture of 2-(*cis*-4-hydroxycyclohexyl)isoindoline-1,3-dione (**15**) (4.0 g, 16.3 mmol), 4-fluorophenol (2.2 g, 19.5 mmol), and triphenylphosphine (6.9 g, 26.1 mmol) in anhydrous THF (50 mL was added DIAD (5.3 g, 26.1 mmol) dropwise, and the reaction mixture was stirred at ambient temperature for 12 h. The reaction was quenched with water, and the aqueous portion was extracted with ethyl acetate. The combined organic layers were washed with brine and dried over anhydrous sodium sulfate. The solid was filtered and the solution was concentrated under reduced pressure. The crude material was purified by chromatography with 60−120 mesh silica column chromatography using 6% EtOAc in petroleum ether as eluent to obtain 2-(*trans*-4-(4-fluorophenoxy)cyclohexyl)isoindoline-1,3-dione (2.8 g, 51%) as a yellow thick liquid. ^1H NMR (400 MHz, $CDCl_3$) δ 7.84 (dd, J = 3.2, 5.7 Hz, 2 H), 7.72 (dd, J = 3.2, 5.7 Hz, 2 H), 6.99−6.95 (m, 2 H), 6.89−6.85 (m, 2 H), 4.23−4.20 (m, 2 H), 2.40−2.37 (m, 2 H), 2.28−2.24 (m, 2 H), 1.85−1.81 (m, 2 H), 1.58−1.55 (m, 2 H); m/z (ESI) 340.2 $(M + H)^+$.

***trans*-4-(4-Fluorophenoxy)cyclohexanamine (17).** To a solution of 2-(*trans*-4-(4-fluorophenoxy)cyclohexyl)isoindoline-1,3-dione (2.8 g, 8.2 mmol) in ethanol (20 mL), was added hydrazine hydrate (1.2 mL, 24.6 mmol), and the reaction mixture was stirred at ambient temperature for 12 h. After completion of the reaction, the resulting precipitate was removed by filtration and the filtrate was dissolved in 5% aqueous HCl (10 mL) and treated with DCM (10 mL). The layers were separated, and the aqueous layer was further basified to pH ≈ 8−9 by using 10% $NaHCO_3$ solution. After basification, the aqueous layer was extracted with DCM and the combined extracts were concentrated

dx.doi.org/10.1021/jm401317z | *J. Med. Chem.* 2013, 56, 10003−10015

to give *trans*-4-(4-fluorophenoxy)cyclohexanamine (1.5 g, 95%) as a colorless oil. ^{1}H NMR (400 MHz, $CDCl_3$) δ 6.92−7.01 (m, 2H), 6.79−6.89 (m, 2H), 4.09 (tt, J = 4.1, 10.4 Hz, 1H), 2.82 (tt, J = 4.0, 10.6 Hz, 1H), 2.04−2.19 (m, 2H), 1.90−2.04 (m, 2H), 1.41−1.58 (m, 2H), 1.10−1.35 (m, 3H); m/z (ESI) 210.2 $(M + H)^+$.

***tert*-Butyl 3-((4-Oxo-3,4-dihydroquinazolin-2-yl)thio)-propanoate (20).** To a mixture of 2-mercaptoquinazolin-4(3*H*)-one (2.50 g, 14.0 mmol) and potassium carbonate (3.88 g, 28.1 mmol) in acetone (70 mL) was added *tert*-butyl 3-bromopropionate (3.52 g, 16.8 mmol). The mixture was stirred at 60 °C for 6 h. The solid was filtered off, and the solution was concentrated. The crude material was purified by chromatography through a Redi-Sep prepacked silica gel column (80 g, eluting with a gradient of 0−40% EtOAc in hexane) to provide *tert*-butyl 3-((4-oxo-3,4-dihydroquinazolin-2-yl)thio)-propanoate (1.18 g, 28% yield) as a white solid. ^{1}H NMR (400 MHz, DMSO-d_6) δ 12.53 (br s, 1 H), 8.04 (dd, J = 7.9, 1.3 Hz, 1 H), 7.77 (ddd, J = 8.3, 7.0, 1.7 Hz, 1 H), 7.53 (d, J = 7.9 Hz, 1 H), 7.43 (td, J = 7.5, 1.2 Hz, 1 H), 3.39 (t, J = 6.8 Hz, 2 H), 2.73 (t, J = 6.8 Hz, 2 H), 1.42 (s, 9 H); m/z (ESI) 307.2 $(M + H)^+$.

3-((4-Oxo-3,4-dihydroquinazolin-2-yl)thio)propanoic Acid (21). To a mixture of *tert*-butyl 3-((4-oxo-3,4-dihydroquinazolin-2-yl)thio)propanoate (0.49 g, 1.6 mmol) in DCM (8.0 mL) was added trifluoroacetic acid (0.36 mL, 4.8 mmol). The mixture was stirred at room temperature for 6 h. The solvent and extra trifluoroacetic acid were evaporated to give 3-((4-oxo-3,4-dihydroquinazolin-2-yl)thio)-propanoic acid (0.39 g, 97% yield) as an off-white solid. ^{1}H NMR (400 MHz, DMSO-d_6) δ 7.87−8.05 (m, 1 H), 7.58−7.76 (m, 1 H), 7.38−7.52 (m, 1 H), 7.34 (ddd, J = 8.0, 7.1, 1.2 Hz, 1 H), 3.29 (t, J = 6.9 Hz, 2 H), 2.66 (t, J = 6.9 Hz, 2 H); m/z (ESI) 251.2 $(M + H)^+$.

General Procedure A for the Synthesis of Tankyrase Inhibitors. To a vial charged with carboxylic acid (0.9 mmol) and amine (0.9 mmol) in DMF (1.0 mL) was added HATU (0.9 mmol). The reaction mixture was stirred at 60 °C overnight. The crude mixture was purified by chromatography through a Redi-Sep prepacked silica gel column (12 g, eluting with a gradient of 0−60% DCM−MeOH−NH_4OH (90:10:1)−DCM) to provide the desired product.

***N*-(2-Methoxyphenyl)-4-(3-(4-oxo-3,4-dihydroquinazolin-2-yl)propanamido)benzamide (8).** ^{1}H NMR (400 MHz, DMSO-d_6) δ 12.27 (br s, 1 H), 10.38 (s, 1 H), 9.28 (s, 1 H), 8.09 (dd, J = 8.0, 1.1 Hz, 1 H), 7.92 (d, J = 8.8 Hz, 2 H), 7.69−7.83 (m, 4 H), 7.56 (d, J = 7.73 Hz, 1 H), 7.43−7.51 (m, 1 H), 7.17 (td, J = 7.7, 1.7 Hz, 1 H), 7.09 (dd, J = 8.4, 1.3 Hz, 1 H), 6.96 (td, J = 7.7, 1.4 Hz, 1 H), 3.84 (s, 3 H), 2.96 (dq, J = 10.8, 5.2 Hz, 4 H); m/z (ESI) 443.2 $(M + H)^+$.

***N*-(2-Methoxy-6-methylphenyl)-4-(3-(4-oxo-3,4-dihydroquinazolin-2-yl)propanamido)benzamide 2,2,2-Trifluoroacetate (23).** ^{1}H NMR (500 MHz, DMSO-d_6) δ 12.22 (br s, 1 H), 10.29 (s, 1 H), 9.38 (s, 1 H), 8.09 (dd, J = 1.2, 7.9 Hz, 1 H), 7.94 (d, J = 8.3 Hz, 2 H), 7.80−7.73 (m, 1 H), 7.70 (d, J = 8.7 Hz, 2 H), 7.56 (d, J = 8.0 Hz, 1 H), 7.48−7.43 (m, 1 H), 7.17 (t, J = 7.9 Hz, 1 H), 6.90 (d, J = 8.1 Hz, 1 H), 6.86 (d, J = 7.7 Hz, 1 H), 3.73 (s, 3 H), 3.01−2.90 (m, 4 H), 2.14 (s, 3 H); m/z (ESI) 457.2 $(M + H)^+$.

***N*-(2-Methoxyphenyl)-2-methyl-4-((3-(4-oxo-3,4-dihydro-2-quinazolinyl)propanoyl)amino)benzamide (24).** ^{1}H NMR (400 MHz, DMSO-d_6) δ 12.26 (s, 1 H), 10.19 (s, 1 H), 9.09 (s, 1 H), 8.09 (dd, J = 1.1, 7.9 Hz, 1 H), 7.85 (d, J = 6.7 Hz, 1 H), 7.77 (ddd, J = 1.6, 7.0, 8.3 Hz, 1 H), 7.55 (d, J = 7.6 Hz, 1 H), 7.52−7.42 (m, 4 H), 7.17−7.11 (m, 1 H), 7.09−7.04 (m, 1 H), 6.98−6.91 (m, 1 H), 3.81 (s, 3 H), 3.00−2.86 (m, 4 H), 2.39 (s, 3 H); m/z (ESI) 457.2 $(M + H)^+$.

***N*-(2-Methoxyphenyl)-*N*-methyl-4-(3-(4-oxo-3,4-dihydroquinazolin-2-yl)propanamido)benzamide 2,2,2-Trifluoroacetate (25).** ^{1}H NMR (500 MHz, DMSO-d_6) δ 10.04 (s, 1 H), 8.07 (dd, J = 1.1, 8.0 Hz, 1 H), 7.78−7.72 (m, 1 H), 7.52 (d, J = 8.0 Hz, 1 H), 7.49−7.42 (m, 1 H), 7.36 (d, J = 8.3 Hz, 2 H), 7.20−7.09 (m, 4 H), 6.94 (d, J = 8.0 Hz, 1 H), 6.83 (t, J = 7.2 Hz, 1 H), 3.68 (s, 3 H), 3.19 (s, 3 H), 2.95−2.88 (m, 2 H), 2.86−2.78 (m, 2 H); m/z (ESI) 457.2 $(M + H)^+$.

***N*-(4-(*N*-(2-Methoxyphenyl)sulfamoyl)phenyl)-3-(4-oxo-3,4-dihydroquinazolin-2-yl)propanamide (26).** ^{1}H NMR (500 MHz, DMSO-d_6) δ 12.19 (br s, 1H), 10.37 (s, 1H), 9.21 (dd, J = 1.23, 9.6 Hz, 1H), 8.08 (d, J = 8.9 Hz, 1H), 7.75 (t, J = 7.0 Hz, 1H), 7.68 (d, J = 9.0 Hz, 2H), 7.61 (d, J = 8.9 Hz, 2H), 7.52 (d, J = 7.8 Hz, 1H), 7.45 (t, J = 7.6 Hz, 1H), 7.19 (dd, J = 1.6, 7.8 Hz, 1H), 7.00−7.12 (m, 1H), 6.77−6.94 (m, 2H), 3.50 (s, 3H), 2.94 (d, J = 5.7 Hz, 2H), 2.90 (d, J = 6.1 Hz, 2H); m/z (ESI) 479.0 $(M + H)^+$.

***N*-(4-(1-Methyl-1*H*-indazol-3-yl)phenyl)-3-(4-oxo-3,4-dihydroquinazolin-2-yl)propanamide (27).** ^{1}H NMR (400 MHz, DMSO-d_6) δ 12.27 (s, 1H), 10.22 (s, 1H), 8.02−8.16 (m, 2H), 7.91 (d, J = 8.9 Hz, 2H), 7.71−7.81 (m, 3H), 7.68 (d, J = 8.5 Hz, 1H), 7.58 (d, J = 7.7 Hz, 1H), 7.40−7.51 (m, 2H), 7.17−7.27 (m, 1H), 4.09 (s, 3H), 2.95 (dd, J = 6.2, 17.8 Hz, 4H); m/z (ESI) 424.5 $(M + H)^+$.

***N*-(4-(1-Methyl-1*H*-benzo[*d*]imidazol-2-yl)phenyl)-3-(4-oxo-3,4-dihydroquinazolin-2-yl)propanamide (28).** ^{1}H NMR (400 MHz, DMSO-d_6) δ 10.59 (s, 1H), 8.04−8.18 (m, 1H), 8.00 (d, J = 7.1 Hz, 1H), 7.87−7.97 (m, 4H), 7.71−7.87 (m, 2H), 7.52−7.68 (m, 3H), 7.48 (ddd, J = 1.2, 7.1, 8.0 Hz, 1H), 4.03 (s, 3H), 3.00 (t, J = 3.3 Hz, 4H); m/z (ESI) 424.5 $(M + H)^+$.

***N*-(4-(Benzo[*d*]oxazol-2-yl)phenyl)-3-(4-oxo-3,4-dihydroquinazolin-2-yl)propanamide (29).** ^{1}H NMR (400 MHz, DMSO-d_6) δ 8.09−8.18 (m, 2H), 7.94−8.07 (m, 3H), 7.78 (dtd, J = 1.7, 3.1, 4.6 Hz, 2H), 7.52 (t, J = 7.5 Hz, 1H), 7.34−7.46 (m, 3H), 7.15−7.26 (m, 1H), 2.84−2.94 (m, 2H), 2.73−2.84 (m, 2H); m/z (ESI) 411.3 $(M + H)^+$.

3-(4-Oxo-3,4-dihydroquinazolin-2-yl)-*N*-(4-(2-phenyl-1*H*-imidazol-5-yl)phenyl)propanamide (30). ^{1}H NMR (400 MHz, DMSO-d_6) δ 12.29 (br s, 1H), 10.29 (s, 1H), 8.02−8.14 (m, 4H), 7.81−7.88 (m, 2H), 7.78 (ddd, J = 1.6, 7.0, 8.3 Hz, 1H), 7.70−7.75 (m, J = 8.6 Hz, 2H), 7.63 (d, J = 7.5 Hz, 3H), 7.57 (d, J = 7.6 Hz, 1H), 7.43−7.51 (m, 1H), 2.95 (dd, J = 5.3, 13.4 Hz, 4H); m/z (ESI) 437.1 $(M + H)^+$.

3-(4-Oxo-3,4-dihydroquinazolin-2-yl)-*N*-(4-(2-phenyl-1*H*-imidazol-5-yl)phenyl)propanamide (31). ^{1}H NMR (400 MHz, DMSO-d_6) δ 10.21 (s, 1H), 8.10 (dd, J = 1.2, 7.9 Hz, 1H), 7.89−7.94 (m, 2H), 7.85 (dd, J = 1.2, 8.3 Hz, 2H), 7.75−7.79 (m, 1H), 7.72 (d, J = 2.1 Hz, 1H), 7.70 (s, 1H), 7.68 (s, 1H), 7.57 (d, J = 7.6 Hz, 1H), 7.44−7.48 (m, 1H), 7.34−7.40 (m, 2H), 7.16−7.24 (m, 1H), 2.95 (dd, J = 6.1, 16.6 Hz, 4H); m/z (ESI) 437.4 $(M + H)^+$.

3-(4-Oxo-3,4-dihydroquinazolin-2-yl)-*N*-(4-(2-phenylthiazol-4-yl)phenyl)propanamide (32). ^{1}H NMR (400 MHz, DMSO-d_6) δ 10.23 (s, 1H), 8.08−8.13 (m, 1H), 8.07 (s, 1H), 7.95−8.05 (m, 4H), 7.78 (ddd, J = 1.6, 7.0, 8.3 Hz, 1H), 7.67−7.74 (m, 2H), 7.56−7.60 (m, 1H), 7.50−7.56 (m, 3H), 7.47 (ddd, J = 1.2, 7.1, 8.0 Hz, 1H), 2.95 (dd, J = 6.3, 17.1 Hz, 4H); m/z (ESI) 453.3 $(M + H)^+$.

3-(4-Oxo-3,4-dihydroquinazolin-2-yl)-*N*-(4-(3-phenyl-1,2,4-oxadiazol-5-yl)phenyl)propanamide (33). ^{1}H NMR (400 MHz, DMSO-d_6) δ 12.28 (s, 1H), 10.55 (s, 1H), 8.12−8.17 (m, 2H), 8.06−8.12 (m, 3H), 7.85−7.92 (m, 2H), 7.77 (ddd, J = 1.6, 7.0, 8.3 Hz, 1H), 7.57−7.65 (m, 3H), 7.54−7.57 (m, 1H), 7.47 (ddd, J = 1.2, 7.1, 8.0 Hz, 1H), 2.98 (t, J = 4.2 Hz, 4H); m/z (ESI) 438.3 $(M + H)^+$.

3-(4-Oxo-3,4-dihydroquinazolin-2-yl)-*N*-(4-(5-phenyl-1,3,4-oxadiazol-2-yl)phenyl)propanamide (34). ^{1}H NMR (400 MHz, DMSO-d_6) δ 12.29 (s, 1 H), 10.48 (s, 1 H), 8.05−8.18 (m, 5 H), 7.82−7.88 (m, 2 H), 7.77 (ddd, J = 8.3, 7.0, 1.6 Hz, 1 H), 7.60−7.68 (m, 3 H), 7.56 (d, J = 7.6 Hz, 1 H), 7.44−7.50 (m, 1 H), 2.97 (dd, J = 7.3, 4.3 Hz, 4 H); m/z (ESI) 438.3 $(M + H)^+$.

***trans*-*N*-(2-Methoxyphenyl)-4-(3-(4-oxo-3,4-dihydroquinazolin-2-yl)propanamido)cyclohexanecarboxamide (35).** ^{1}H NMR (400 MHz, DMSO-d_6) δ 12.18 (br s, 1 H), 8.95 (s, 1 H), 8.08 (dd, J = 1.1, 8.0 Hz, 1 H), 7.97−7.90 (m, 1 H), 7.86 (d, J = 7.9 Hz, 1 H), 7.77 (ddd, J = 1.6, 7.0, 8.3 Hz, 1 H), 7.58−7.53 (m, 1 H), 7.46 (ddd, J = 1.2, 7.1, 8.0 Hz, 1 H), 7.08−6.97 (m, 2 H), 6.91−6.83 (m, 1 H), 3.82 (s, 3 H), 3.56−3.43 (m, 1 H), 2.87−2.81 (m, 2 H), 2.58 (t, J = 7.4 Hz, 2 H), 2.49−2.42 (m, 1 H), 1.82 (d, J = 11.2 Hz, 4 H), 1.51−1.36 (m, 2 H), 1.27−1.12 (m, 2 H). m/z (ESI) 449.2 $(M + H)^+$.

***cis*-*N*-(2-Methoxyphenyl)-4-(3-(4-oxo-3,4-dihydroquinazolin-2-yl)propanamido)cyclohexanecarboxamide (36).** ^{1}H NMR (500 MHz, DMSO-d_6) δ 12.13 (s, 1 H), 8.83 (s, 1 H), 8.07 (d, J = 8.4 Hz, 1 H), 7.94 (d, J = 7.3 Hz, 1 H), 7.89 (d, J = 7.4 Hz, 1 H), 7.77−7.72 (m, 1 H), 7.56 (d, J = 8.3 Hz, 1 H), 7.44 (t, J = 7.6 Hz, 1 H), 7.08−7.00 (m, 1 H), 6.93−6.87 (m, 1 H), 3.82 (s, 3 H), 2.88−2.82 (m, 2 H), 2.68−2.62 (m, 2 H), 2.55 (br s, 2 H), 1.83 (d, J = 10.6 Hz, 2 H), 1.72−1.63 (m, 2 H), 1.63−1.47 (m, 4 H); m/z (ESI) 449.2 $(M + H)^+$.

3-(4-Oxo-3,4-dihydro-2-quinazolinyl)-*N*-(*trans*-4-(5-phenyl-1,3,4-oxadiazol-2-yl)cyclohexyl)propanamide (37). ^{1}H NMR (400 MHz, DMSO-d_6) δ 12.19 (s, 1 H), 8.09 (dd, J = 1.2, 8.0 Hz, 1 H), 7.96−8.03 (m, 2 H), 7.93 (d, J = 7.7 Hz, 1 H), 7.78 (ddd, J = 1.6, 7.0, 8.3 Hz, 1 H), 7.54−7.66 (m, 4 H), 7.43−7.51 (m, 1 H), 3.53−3.68 (m, 1 H), 3.00 (tt, J = 3.5, 11.9 Hz, 1 H), 2.86 (t, J = 7.3 Hz, 2 H), 2.61 (t, J = 7.4 Hz, 2 H), 2.17 (d, J = 11.4 Hz, 2 H), 1.91 (dd, J = 3.1, 13.0 Hz, 2 H), 1.64 (dq, J = 2. 9, 12.8 Hz, 2 H), 1.26−1.44 (m, 2 H); m/z (ESI) 444.2 (M + H)$^+$.

General Procedure B for the Synthesis of Tankyrase Inhibitors. To a vial charged with amine (0.28 mmol) in DMF (1.0 mL) were added triethylamine (0.12 mL, 0.84 mmol), carboxylic acid (0.28 mmol), and 1-propanephosphonic acid cyclic anhydride (50+% solution in DMF) (0.18 mL, 0.28 mmol). The reaction mixture was stirred at room temperature overnight. The crude mixture was purified by chromatography through a Redi-Sep prepacked silica gel column (12 g, eluting with a gradient of 0−60% DCM−MeOH−NH_4OH (90:10:1)−DCM) to provide the desired product.

3-((4-Oxo-3,4-dihydroquinazolin-2-yl)thio)-*N*-(*trans*-4-(5-phenyl-1,3,4-oxadiazol-2-yl)cyclohexyl)propanamide (22). ^{1}H NMR (400 MHz, DMSO-d_6) δ 12.50 (br s, 1 H), 8.02−8.09 (m, 1 H), 7.96−8.02 (m, 2 H), 7.90 (d, J = 7.6 Hz, 1 H), 7.72−7.83 (m, 1 H), 7.57−7.66 (m, 3 H), 7.50−7.57 (m, 1 H), 7.43 (ddd, J = 8.0, 7.1, 1.2 Hz, 1 H), 3.55−3.71 (m, 1 H), 3.41 (t, J = 6.8 Hz, 2 H), 3.00 (tt, J = 11.9, 3.6 Hz, 1 H), 2.56−2.63 (m, 2 H), 2.12−2.24 (m, 2 H), 1.85−2.02 (m, 2 H), 1.56−1.75 (m, 2 H), 1.22−1.44 (m, 2 H); m/z (ESI) 476.2 (M + H)$^+$.

3-(4-Oxo-3,4-dihydropyrido[2,3-*d*]pyrimidin-2-yl)-*N*-(*trans*-4-(5-phenyl-1,3,4-oxadiazol-2-yl)cyclohexyl)propanamide (38). ^{1}H NMR (400 MHz, DMSO-d_6) δ 12.22 (br s, 1 H), 8.66 (dd, J = 4.6, 1.9 Hz, 1 H), 8.22 (dd, J = 7.9, 2.0 Hz, 1 H), 7.72−7.79 (m, 2 H), 7.69 (d, J = 7.7 Hz, 1 H), 7.30−7.43 (m, 3 H), 7.24 (dd, J = 7.8, 4.6 Hz, 1 H), 3.82 (q, J = 5.3 Hz, 1 H), 3.36 (dtd, J = 11.4, 7.5, 7.5, 4.2 Hz, 1 H), 2.66 (t, J = 7.3 Hz, 2 H), 2.41 (t, J = 7.4 Hz, 2 H), 1.81−2.00 (m, 2 H), 1.67 (dd, J = 13.4, 3.6 Hz, 2 H), 1.29−1.49 (m, 2 H), 1.00−1.21 (m, 2 H); m/z (ESI) 445.2 (M + H) .

3-(4-Oxo-3,4,5,6,7,8-hexahydropyrido[2,3-*d*]pyrimidin-2-yl)-*N*-(*trans*-4-(5-phenyl-1,3,4-oxadiazol-2-yl)cyclohexyl)propanamide (39). ^{1}H NMR (400 MHz, DMSO-d_6) δ 11.23 (br s, 1 H), 8.00 (dd, J = 7. 8, 1.7 Hz, 2 H), 7.82 (d, J = 7.6 Hz, 1 H), 7.56−7.68 (m, 3 H), 6.55 (br s, 1 H), 3.52−3.69 (m, 1 H), 3.17 (br s, 2 H), 2.93−3.06 (m, 1 H), 2.55−2.64 (m, 2 H), 2.39−2.49 (m, 2 H), 2.29 (t, J = 6.1 Hz, 2 H), 2.18 (d, J = 12.1 Hz, 2 H), 1.92 (d, J = 10.1 Hz, 2 H), 1.56−1.75 (m, 4 H), 1.30−1.44 (m, 2 H); m/z (ESI) 449.2 (M + H)$^+$.

(*S*)-1-((4-Oxo-3,4-dihydroquinazolin-2-yl)methyl)-*N*-(*trans*-4-(5-phenyl-1,3,4-oxadiazol-2-yl)cyclohexyl)piperidine-3-carboxamide (40). ^{1}H NMR (500 MHz, DMSO-d_6) δ 11.22 (br s, 1 H), 8.11 (d, J = 7.9 Hz, 1 H), 7.94−8.02 (m, 2 H), 7.75−7.87 (m, 2 H), 7.55− 7.70 (m, 4 H), 7.50 (t, J = 7.5 Hz, 1 H), 3.51−3.61 (m, 1 H), 3.45 (s, 2 H), 2.95 (t, J = 12.0 Hz, 1 H), 2.77 (d, J = 11.2 Hz, 2 H), 2.37 (br s, 1 H), 2.26−2.35 (m, 1 H), 2.18−2.26 (m, 1 H), 2.13 (d, J = 15.4 Hz, 2 H), 1.86 (d, J = 13.6 Hz, 2 H), 1.55−1.73 (m, 4 H), 1.51 (d, J = 11.1 Hz, 1 H), 1.35−1.46 (m, 1 H), 1.23−1.35 (m, 2 H); m/z (ESI) 513.3 (M + H)$^+$.

2-((*R*)-1-((4-Oxo-3,4-dihydroquinazolin-2-yl)methyl)-pyrrolidin-2-yl)-*N*-(*trans*-4-(5-phenyl-1,3,4-oxadiazol-2-yl)-cyclohexyl)acetamide (41). ^{1}H NMR (500 MHz, DMSO-d_6) δ 11.75 (br s, 1 H), 8.08−8.16 (m, 1 H), 7.94−8.04 (m, 3 H), 7.75−7.85 (m, 1 H), 7.55−7.66 (m, 4 H), 7.49 (t, J = 7.6 Hz, 1 H), 3.94 (d, J = 14.6 Hz, 1 H), 3.55−3.69 (m, 1 H), 3.39 (d, J = 14.6 Hz, 1 H), 2.89−3.04 (m, 3 H), 2.33−2.44 (m, 2 H), 2.22 (dd, J = 13.7, 6.9 Hz, 1 H), 2.15 (t, J = 12.7 Hz, 2 H), 1.81−1.98 (m, 3 H), 1.51−1.74 (m, 5 H), 1.23−1.45 (m, 2 H); m/z (ESI) 513.3 (M + H)$^+$.

2-((4-Oxo-3,4-dihydroquinazolin-2-yl)thio)-*N*-(*trans*-4-(5-phenyl-1,3,4-oxadiazol-2-yl)cyclohexyl)acetamide (42). ^{1}H NMR (400 MHz, DMSO-d_6) δ 12.53 (br s, 1 H), 8.14 (d, J = 7.5 Hz, 1 H), 7.80−8.00 (m, 3 H), 7.66 (t, J = 7.0 Hz, 1 H), 7.48 (d, J = 6.9 Hz, 4 H) 7.40 (d, J = 8.12 Hz, 1 H) 7.31 (t, J = 7.2 Hz, 1 H), 3.82 (s, 2 H), 3.51 (d, J = 6.8 Hz, 1 H), 2.80−2.98 (m, 1 H), 2.05 (d, J = 11.2 Hz, 2 H), 1.82 (d, J = 10.8 Hz, 2 H), 1.41−1.62 (m, 2 H), 1.16−1.40 (m, 2 H); m/z (ESI) 462.2 (M + H)$^+$.

4-(4-Oxo-3,4-dihydro-2-quinazolinyl)-*N*-(*trans*-4-(5-phenyl-1,3,4-oxadiazol-2-yl)cyclohexyl)butanamide (43). ^{1}H NMR (400 MHz, DMSO-d_6) δ 12.16 (br s, 1 H), 8.08 (dd, J = 7.92, 1.4 Hz, 1 H), 7.95−8.03 (m, 2 H), 7.78 (td, J = 7.7, 1.6 Hz, 2 H), 7.54−7.68 (m, 4 H), 7.41−7.51 (m, 1 H), 3.51−3.66 (m, 1 H), 2.90−3.05 (m, 1 H), 2.61 (t, J = 7.5 Hz, 2 H), 2.15 (t, J = 7.34 Hz, 4 H), 1.85−2.03 (m, 4 H), 1.54−1.72 (m, 2 H), 1.22−1.41 (m, 2 H); m/z (ESI) 458.2 (M + H)$^+$.

4-((4-Oxo-3,4-dihydroquinazolin-2-yl)thio)-*N*-(*trans*-4-(5-phenyl-1,3,4-oxadiazol-2-yl)cyclohexyl)butanamide (44). ^{1}H NMR (400 MHz, DMSO-d_6) δ 12.52 (br s, 1 H), 7.93−8.08 (m, 3 H), 7.82 (d, J = 7.6 Hz, 1 H), 7.76 (t, J = 7.5 Hz, 1 H), 7.55−7.66 (m, 3 H), 7.52 (d, J = 8.0 Hz, 1 H), 7.41 (t, J = 7.5 Hz, 1 H), 3.61 (d, J = 7.8 Hz, 1 H), 3.19−3.27 (m, 2 H), 2.90−3.05 (m, 1 H), 2.23 (t, J = 7.1 Hz, 2 H), 2.16 (d, J = 12.5 Hz, 2 H), 1.84−2.01 (m, 4 H), 1.55−1.73 (m, 2 H), 1.26−1.43 (m, 2 H); m/z (ESI) 490.2 (M + H)$^+$.

3-((4-Oxo-3,4,5,6,7,8-hexahydroquinazolin-2-yl)thio)-*N*-(*trans*-4-(5-phenyl-1,3,4-oxadiazol-2-yl)cyclohexyl)-propanamide (45). ^{1}H NMR (400 MHz, DMSO-d_6) δ 12.40 (br s, 1 H), 8.00 (dd, J = 7. 8, 1.7 Hz, 2 H), 7.86 (d, J = 7.5 Hz, 1 H), 7.52−7.67 (m, 3 H), 3.62 (d, J = 7.8 Hz, 1 H), 3.21−3.29 (m, 2 H), 3.00 (t, J = 11.8 Hz, 1 H), 2.29 (br s, 2 H), 2.18 (d, J = 12.6 Hz, 2 H), 1.93 (d, J = 10.4 Hz, 2 H), 1.54−1.77 (m, 6 H), 1.24−1.43 (m, 2 H); m/z (ESI) 480.2 (M + H)$^+$.

3-((6-Oxo-1,6-dihydropyrimidin-2-yl)thio)-*N*-(*trans*-4-(5-phenyl-1,3,4-oxadiazol-2-yl)cyclohexyl)propanamide (46). ^{1}H NMR (400 MHz, DMSO-d_6) δ 12.65 (br s, 1 H), 8.00 (dd, J = 7.8, 1.7 Hz, 2 H), 7.89 (d, J = 7.5 Hz, 2 H), 7.53−7.69 (m, 4 H), 6.10 (br s, 1 H), 3.62 (dd, J = 7.4, 4.2 Hz, 1 H), 3.00 (t, J = 11.9 Hz, 1 H), 2.18 (d, J = 12.0 Hz, 2 H), 1.84−2.00 (m, 2 H), 1.58−1.74 (m, 2 H), 1.27−1.45 (m, 2 H); m/z (ESI) 426.2 (M + H)$^+$.

***N*-(*trans*-4-(4-Fluorophenoxy)cyclohexyl)-3-((4-oxo-3,4-dihydroquinazolin-2-yl)thio)propanamide (47).** ^{1}H NMR (400 MHz, DMSO-d_6) δ 12.50 (br s, 1 H), 8.04 (dd, J = 8.0, 1.2 Hz, 1 H), 7.85 (d, J = 7.6 Hz, 1 H), 7.77 (td, J = 7.68, 1.6 Hz, 1 H), 7.54 (d, J = 8.2 Hz, 1 H), 7.39−7.46 (m, 1 H), 7.05−7.12 (m, 2 H), 6.92−6.99 (m, 2 H), 4.15−4.30 (m, 1 H), 3.54−3.68 (m, 1 H), 3.40 (t, J = 6.8 Hz, 2 H), 2.55−2.62 (m, 2 H), 1.99−2.08 (m, 2 H), 1.79−1.89 (m, 2 H), 1.23−1.48 (m, 4 H); m/z (ESI) 442.2 (M + H)$^+$.

***N*-(*trans*-4-(4-Chlorophenoxy)cyclohexyl)-3-((4-oxo-3,4-dihydroquinazolin-2-yl)thio)propanamide (48).** ^{1}H NMR (400 MHz, DMSO-d_6) δ 12.50 (br s, 1 H), 8.04 (dd, J = 8.0, 1.2 Hz, 1 H), 7.86 (d, J = 7.4 Hz, 1 H), 7.73−7.81 (m, 1 H), 7.54 (d, J = 8.3 Hz, 1 H), 7.38−7.46 (m, 1 H), 7.25−7.33 (m, 2 H), 6.94−7.01 (m, 2 H), 4.28 (t, J = 4.3 Hz, 1 H), 3.53−3.67 (m, 1 H), 3.40 (t, J = 6.8 Hz, 2 H), 2.55−2.62 (m, 2 H), 2.03 (d, J = 9.8 Hz, 2 H), 1.85 (d, J = 9.7 Hz, 2 H), 1.24−1.52 (m, 4 H); m/z (ESI) 458.2 (M + H)$^+$.

***N*-(*trans*-4-(4-Cyanophenoxy)cyclohexyl)-3-((4-oxo-3,4-dihydroquinazolin-2-yl)thio)propanamide (49).** ^{1}H NMR (400 MHz, DMSO-d_6) δ 12.31 (s, 1 H), 7.85 (dd, J = 7 0.9, 1.2 Hz, 1 H), 7.69 (d, J = 7.5 Hz, 1 H), 7.50−7.62 (m, 3 H), 7.35 (d, J = 8.1 Hz, 1 H), 7.20−7.27 (m, 1 H), 6.91−6.97 (m, 2 H), 4.21−4.34 (m, 1 H), 3.37−3.51 (m, 1 H), 3.21 (t, J = 6.7 Hz, 2 H), 2.40 (t, J = 6.8 Hz, 2 H), 1.87 (d, J = 9.7 Hz, 2 H), 1.60−1.74 (m, 2 H), 1.09−1.35 (m, 4 H); m/z (ESI) 449.2 (M + H)$^+$.

3-((4-Oxo-3,4-dihydroquinazolin-2-yl)thio)-*N*-(*trans*-4-(pyridin-4-yloxy)cyclohexyl)propanamide (50). ^{1}H NMR (400 MHz, DMSO-d_6) δ 12.50 (br s, 1 H), 8.35 (d, J = 6.2 Hz, 2 H), 8.04 (d, J = 6.9 Hz, 1 H), 7.88 (d, J = 7.6 Hz, 1 H), 7.77 (t, J = 6.9 Hz, 1 H), 7.53 (d, J = 7.9 Hz, 1 H), 7.42 (t, J = 7.3 Hz, 1 H), 6.97 (d, J = 6.0 Hz, 2 H), 4.34−4.54 (m, 1 H), 3.63 (d, J = 6.3 Hz, 1 H), 3.40 (t, J = 6.5 Hz, 2 H), 2.59 (t, J = 6.8 Hz, 2 H), 2.06 (d, J = 9.9 Hz, 2 H), 1.86 (d, J = 9.3 Hz, 2 H), 1.29−1.54 (m, 4 H); m/z (ESI) 425.2 (M + H)$^+$.

3-((4-Oxo-3,4-dihydroquinazolin-2-yl)thio)-*N*-(*trans*-4-(pyridin-2-yloxy)cyclohexyl)propanamide (51). ^{1}H NMR (400 MHz, DMSO-d_6) δ 12.50 (br s, 1 H), 8.10−8.18 (m, 1 H), 8.04 (dd, J = 7.9, 1.2 Hz, 1 H), 7.85 (d, J = 7.7 Hz, 1 H), 7.77 (ddd, J = 8.3, 7.0, 1.6 Hz, 1 H), 7.63−7.73 (m, 1 H), 7.54 (d, J = 7.9 Hz, 1 H), 7.37−7.50 (m, 1 H), 6.93 (ddd, J = 7.09, 5.0, 0.9 Hz, 1 H), 6.75 (dt, J = 8.4, 0.9 Hz, 1 H), 4.80−5.02 (m, 1 H), 3.53−3.71 (m, 1 H), 3.40 (t, J = 6.7 Hz, 2

H), 2.54−2.63 (m, 2 H), 2.01−2.13 (m, 2 H), 1.77−1.93 (m, 2 H), 1.39−1.56 (m, 2 H), 1.23−1.39 (m, 2 H); *m/z* (ESI) 425.2 $(M + H)^+$.

***N*-(*trans*-4-(3-Chlorophenoxy)cyclohexyl)-3-((4-oxo-3,4-dihydroquinazolin-2-yl)thio)propanamide (52).** ^{1}H NMR (400 MHz, DMSO-d_6) δ 12.55 (br s, 1 H), 8.09 (dd, *J* = 7.9, 1.1 Hz, 1 H), 7.91 (d, *J* = 7.6 Hz, 1 H), 7.82 (ddd, *J* = 8.3, 7.0, 1.6 Hz, 1 H), 7.59 (d, *J* = 8.1 Hz, 1 H), 7.48 (ddd, *J* = 8.0, 7.1, 1.1 Hz, 1 H), 7.34 (t, *J* = 8.2 Hz, 1 H), 7.05−7.13 (m, 1 H), 7.00 (ddd, *J* = 10.9, 8.2, 0.8 Hz, 1 H), 7.00 (ddd, *J* = 15.3, 8.2, 0.8 Hz, 1 H), 4.41 (s, 1 H), 3.45 (t, *J* = 6.7 Hz, 2 H), 2.60−2.68 (m, 2 H), 1.99−2.16 (m, 2 H), 1.83−1.99 (m, 2 H), 1.29−1.57 (m, 4 H); *m/z* (ESI) 458.2 $(M + H)^+$.

3-((4-Oxo-3,4-dihydroquinazolin-2-yl)thio)-*N*-(*trans*-4-(3-cyanophenoxy)cyclohexyl)propanamide (53). ^{1}H NMR (400 MHz, DMSO-d_6) δ 12.49 (s, 1 H), 8.03 (dd, *J* = 1.3, 7.9 Hz, 1 H), 7.86 (d, *J* = 7.3 Hz, 1 H), 7.76 (dt, *J* = 1.6, 7.7 Hz, 1 H), 7.53 (d, *J* = 7.92 Hz, 1 H), 7.38−7.49 (m, 3 H), 7.35 (td, *J* = 1.2, 7.7 Hz, 1 H), 7.29 (ddd, *J* = 1.0, 2.6, 8.4 Hz, 1 H), 4.33−4.49 (m, 1 H), 3.55−3.67 (m, 1 H), 3.36−3.42 (m, 2 H), 2.58 (t, *J* = 6.7 Hz, 2 H), 2.00−2.09 (m, 2 H), 1.79−1.90 (m, 2 H), 1.28−1.50 (m, 4 H); *m/z* (ESI) 449.2 $(M + H)^+$.

***N*-(*trans*-4-(4-Chloro-3-cyanophenoxy)cyclohexyl)-3-((4-oxo-3,4-dihydroquinazolin-2-yl)thio)propanamide (54).** ^{1}H NMR (400 MHz, DMSO-d_6) δ 12.50 (br s, 1 H), 8.04 (dd, *J* = 7.9, 1.1 Hz, 1 H), 7.87 (d, *J* = 7.5 Hz, 1 H), 7.73−7.81 (m, 1 H), 7.64 (d, *J* = 3.0 Hz, 1 H), 7.60 (d, *J* = 9.0 Hz, 1 H), 7.54 (d, *J* = 8.0 Hz, 1 H), 7.38−7.47 (m, 1 H), 7.32 (dd, *J* = 9.0, 3.0 Hz, 1 H), 4.35−4.50 (m, 1 H), 3.55−3.69 (m, 1 H), 3.40 (t, *J* = 6.7 Hz, 2 H), 2.59 (t, *J* = 6.9 Hz, 2 H), 2.04 (d, *J* = 10.1 Hz, 2 H), 1.85 (d, *J* = 9.7 Hz, 2 H), 1.28−1.50 (m, 4 H); *m/z* (ESI) 483.2 $(M + H)^+$.

***N*-(*trans*-4-(3-Chloro-4-cyanophenoxy)cyclohexyl)-3-((4-oxo-3,4-dihydroquinazolin-2-yl)thio)propanamide (55).** ^{1}H NMR (400 MHz, DMSO-d_6) δ 12.51 (s, 1 H), 8.04 (dt, *J* = 7.9, 0.8 Hz, 1 H), 7.81−7.92 (m, 2 H), 7.77 (ddd, *J* = 8.3, 7.0, 1.6 Hz, 1 H), 7.54 (d, *J* = 8.0 Hz, 1 H), 7.43 (ddd, *J* = 8.0, 7.1, 1.17 Hz, 1 H), 7.37 (d, *J* = 2.5 Hz, 1 H), 7.13 (dd, *J* = 8.9, 2.5 Hz, 1 H), 4.43−4.65 (m, 1 H), 3.52−3.71 (m, 1 H), 3.40 (t, *J* = 6.7 Hz, 2 H), 2.54−2.63 (m, 2 H), 2.05 (d, *J* = 10.2 Hz, 2 H), 1.76−1.92 (m, 2 H), 1.27−1.56 (m, 4 H); *m/z* (ESI) 483.2 $(M + H)^+$.

■ ASSOCIATED CONTENT

Ⓢ Supporting Information

Synthesis of key intermediates leading to compounds **8**, **23**, **24**, **35**, **38**, **39**, **42**, and **44**−**46**; Figure S1 showing the dihedral scan calculation of sulfur ethylene linker and three-carbon linker. This material is available free of charge via the Internet at http://pubs.acs.org.

■ AUTHOR INFORMATION

Corresponding Authors

*Z.H.: phone, 617-444-5233; e-mail, zihao.hua@amgen.com.
*E.F.D.: phone, 617-444-5189; e-mail, erin.dimauro@amgen.com.

Notes

The authors declare no competing financial interest.

■ ACKNOWLEDGMENTS

The authors thank Dhan Bagal, Matthew Potter, Paul H. Krolikowski, Grace Bi, and Shawn Ayube for analytical support, and Dr. Margaret Chu-Moyer for proof-reading the manuscript.

■ ABBREVIATIONS USED

TNKS, tankyrase; APC, adenomatous polyposis coli; axin, axis inhibition protein; GSK3β, glycogen synthase kinase 3β; CK1α, casein kinase 1α; PARP, poly ADP-ribose polymerase; CRC, colorectal cancer; NAD, nicotinamide adenine dinucleotide; TRF1, telomere repeating binding factor 1; IWR, inhibitor of Wnt response; TBC, total β-catenin; SIF, simulated intestinal fluid; DIPEA, diisopropylethylamine; HATU, *O*-(7-azabenzotriazol-1-yl)-*N*,*N*,*N*′,*N*′-tetramethyluronium hexafluorophosphte; DIAD, diisopropyl azodicarboxylate; T3P, propylphosphonic acid anhydride; SAR, structure−activity relationship; LE, ligand efficiency; LipE, lipophilic efficiency; STF, supertop flash; DMSO, dimethylsulfoxide; TFA, trifluoroacetic acid; DCM, dichloromethane; DMF, *N*,*N*-dimethylformamide

■ REFERENCES

(1) Clevers, H. Wnt/β-catenin signaling in development and disease. *Cell* **2006**, *127*, 469−480.
(2) (a) Reya, T.; Clevers, H. Wnt signaling in stem cells and cancer. *Nature* **2005**, *434*, 843. (b) Barker, N.; Clevers, H. Mining the Wnt pathway for cancer therapeutics. *Nat. Rev. Drug Discovery* **2006**, *5*, 997−1014. (c) Polakis, P. The many ways of Wnt in cancer. *Curr. Opin. Genet. Dev.* **2007**, *17*, 45−51.
(3) (a) Martin, S. A.; Lord, C. J.; Ashworth, A. DNA repairs deficiency as a therapeutic target in cancer. *Curr. Opin. Genet. Dev.* **2008**, *18*, 80−86. (b) Jones, P. Development of poly(ADP-ribose)polymerase (PARP) inhibitors in oncology. *Annu. Rep. Med. Chem.* **2010**, *45*, 229−243. (c) Ferraris, D. V. Evolution of poly(ADP-ribose) polymerase-1 (PARP-1) inhibitors. From concept to clinic. *J. Med. Chem.* **2010**, *53*, 4561−4584.
(4) Smith, S.; Giriat, I.; Schmitt, A.; de Lange, T. Tankyrase, a poly(ADP-ribose) polymerase at human telomeres. *Science* **1998**, *282*, 1484−1487.
(5) (a) Riffell, J. L.; Lord, C. J.; Ashworth, A. Tankyrase-targeted therapeutics: expanding opportunities in the PARP family. *Nat. Rev. Drug Discovery* **2012**, *11*, 923−936. (b) Lehtiö, L.; Chi, N.-W.; Krauss, S. Tankyrase as drug targets. *FEBS J.* **2013**, *280*, 3576−3593 and references herein..
(6) Waaler, J.; Ondrej, M.; Lucie, T.; Huyen, D.; Vladimir, K.; Ray, W. S.; Erik, P. J.; Marie, P. N.; Tor, J. E.; Olga, M.; Gradl, D.; Voronkov, A.; von Kries, J. P.; Krauss, S. A novel tankyrase inhibitor decreases canonical Wnt signaling in colon carcinoma cells and reduces tumor growth in conditional APC mutant mice. *Cancer Res.* **2012**, *72* (11), 2822−2832 and references herein..
(7) Huang, S. M.; Mishina, Y. M.; Liu, S.; Cheung, A.; Stegmeier, F.; Michaud, G. A.; Charlat, O.; Wiellette, E.; Zhang, Y.; Wiessner, S.; Hild, M.; Shi, X.; Wilson, C. J.; Mickanin, C.; Myer, V.; Fazal, A.; Tomlinson, R.; Serluca, F.; Shao, W.; Cheng, H.; Shultz, M.; Rau, C.; Schirle, M.; Schlegl, J.; Ghidelli, S.; Fawell, S.; Lu, C.; Curtis, D.; Kirschner, M. W.; Lengauer, C.; Finan, P. M.; Tallarico, J. A.; Bouwmeester, T.; Porter, J. A.; Bauer, A.; Cong, F. Tankyrase inhibition stabilizes axin and antagonizes Wnt signaling. *Nature* **2009**, *46*, 614−620.
(8) (a) Chen, B.; Dodge, M. E.; Tang, W.; Lu, J.; Ma, Z.; Fan, C.-W.; Wei, S.; Hao, W.; Kilgore, J.; Williams, N. S.; Roth, M. G.; Amatruda, J. F.; Chen, C.; Lum, L. Small molecule-mediated disruption of Wnt-dependent signaling in tissue regeneration and cancer. *Nat. Chem. Biol.* **2009**, *5* (2), 100−107. (b) Lu, J.; Ma, Z.; Hsieh, J.-C.; Fan, C.-W.; Chen, B.; Longgood, J. C.; Williams, N. S.; Amatruda, J. F.; Lum, L.; Chen, C. Structure−activity relationship studies of small-molecule inhibitors of Wnt response. *Bioorg. Med. Chem. Lett.* **2009**, *19* (14), 3825−3827.
(9) Karlberg, T.; Markova, N.; Johansson, I.; Hammarstrom, M.; Schutz, P.; Weigelt, J.; Schuler, H. Structural basis for the interaction between tankyrase-2 and potent wnt-signaling inhibitor. *J. Med. Chem.* **2010**, *53*, 5352−5355.
(10) Gunaydin, H.; Gu, Y.; Huang, X. Novel binding mode of a potent and selective tankyrase inhibitor. *PLoS One* **2012**, *7*, e333740.
(11) Narwal, M.; Venkannagari, H.; Lehtiö, L. Structural basis of selective inhibition of human tankyrase. *J. Med. Chem.* **2012**, *55*, 1360−1367.
(12) Waaler, J.; Machon, O.; von Kries, J. P.; Wilson, S. R.; Lundenes, E.; Wedlich, D.; Gradl, D.; Paulsen, J. E.; Machonova, O.; Dembinski, J. L.; Dinh, H.; Krauss, S. Novel synthetic antagonists of canonical Wnt

signaling inhibit colorectal cancer cell growth. *Cancer Res.* **2011**, *71*, 197−205.
(13) Shultz, M. D.; Kirby, C. A.; Stams, T.; Chin, D. N.; Blank, J.; Charlat, O.; Cheng, H.; Cheung, A.; Cong, F.; Feng, Y.; Fortin, P. D.; Hood, T.; Tyagi, V.; Xu, M.; Zhang, B.; Shao, W. [1,2,4]Triazol-3-ylsulfanylmethyl)-3-phenyl-[1,2,4]oxadiazoles: antagonists of the Wnt pathway that inhibit tankyrases 1 and 2 via novel adenosine pocket binding. *J. Med. Chem.* **2012**, *55*, 1127−1136.
(14) Voronkov, A.; Holsworth, D. D.; Waaler, J.; Wilson, S. R.; Ekblad, B.; Perdreau-Dahl, H.; Dinh, G.; Drewes, G.; Hopf, C.; Morth, J. P.; Krauss, S. Structural basis and SAR for G007-LK, a lead stage 1,2,4-triazole based specific tankyrase 1/2 inhibitor. *J. Med. Chem.* **2013**, *56*, 3012−3023.
(15) Lau, T.; Chan, E.; Callow, M.; Waaler, J.; Boggs, J.; Blake, R. A.; Magnuson, S.; Sambrone, A.; Schutten, M.; Firestein, R.; Machon, O.; Korinek, V.; Choo, E.; Diaz, D.; Merchant, M.; Polakis, P.; Holsworth, D. D.; Krauss, S.; Costa, M. A novel tankyrase small-molecule inhibitor suppresses *APC* mutation−driven colorectal tumor growth. *Cancer Res.* **2013**, *73*, 3132−3144.
(16) During the preparation of this manuscript, studies on the identification of different types of tankyrase inhibitor were reported: (a) Narwal, M.; Haikarainen, T.; Fallarero, A.; Vuorela, P. M.; Lehtiö, L. Screening and structural analysis of flavones inhibiting tankyrases. *J. Med. Chem.* **2013**, *56*, 3507−3517. (b) Shultz, M. D.; Cheung, A. K.; Kirby, C. A.; Firestone, B.; Chen, C. H.; Chen, Z.; Chin, D.; DiPietro, L.; Fazal, A.; Feng, Y.; Fortin, P. D.; Gould, T.; Lagu, B.; Lei, H.; Lenoir, F.; Majumdar, D.; Ochala, E.; Palermo, M. G.; Pham, L.; Pu, M.; Smith, T.; Stams, T.; Tomlinson, R. C.; Toure, B. B.; Visser, M.; Wang, R. M.; Waters, N. J.; Shao, W. Identification of NVP-TNKS656: the use of structure−efficiency relationships (SER) to generate a highly potent, selective and orally active tankyrase inhibitor. *J. Med. Chem.* **2013**, *56*, 6495−6511. (c) Shultz, M. D.; Majumdar, D.; Chin, D.; Fortin, P. D.; Feng, Y.; Gould, T.; Kirby, C. A.; Stams, T.; Waters, N. J.; Shao, W. Structure−efficiency relationship of [1,2,4]triazol-3-ylamines as novel nicotinamide isosteres that inhibit tankyrases. *J. Med. Chem.* **2013**, *56*, 7049−7059. (d) Larsson, E. A.; Jansson, A.; Ng, F. M.; Then, S. W.; Panicker, R.; Liu, B.; Sangthongpitag, K.; Pendharkar, V.; Tai, S. J.; Hill, J.; Dan, C.; Ho, S. Y.; Cheong, W. W.; Poulsen, A.; Blanchard, S.; Lin, G. R.; Alam, J.; Keller, T. H.; Nordlund, P. Fragment-based ligand design of novel potent inhibitors of tankyrases. *J. Med. Chem.* **2013**, *56*, 4497−4508. (e) Bregman, H.; Chakka, N.; Guzman-Perez, A.; Gunaydin, H.; Gu, Y.; Huang, X.; Berry, V.; Liu, J.; Teffera, Y.; Huang, L.; Egge, B.; Mullady, E. L.; Schneider, S.; Andrews, P. S.; Mishra, A.; Newcomb, J.; Serafino, R.; Strathdee, C. A.; Turci, S. M.; Wilson, C.; DiMauro, E. F. The discovery of novel, induced-pocket binding oxazolidinones as potent, selective, and orally bioavailable tankyrase inhibitors. *J. Med. Chem.* **2013**, *56*, 4320−4342.
(17) Bregman, H.; Gunaydin, H.; Gu, Y.; Schneider, S.; Wilson, C.; DiMauro, E. F.; Huang, X. Discovery of a class of novel tankyrase inhibitors that bind to both the nicotinamide pocket and the induced pocket. *J. Med. Chem.* **2013**, *56*, 1341−1345.
(18) Plasma stability assay: Lithium heparanized, CD-1 mouse plasma was spiked with 1 μM substrate. The spiked plasma is incubated at 37 °C for 3 h. Aliquots are collected at 0, 0.167, 1, 2, and 3 h (n = 2). The CD-1, lithium heparanized mouse plasma samples were extracted using acetonitrile protein precipitation. Tolbutamide was used as an internal standard. The substrate concentrations were determined by LC−MS/MS using reversed-phase ultraperformance liquid chromatography on an ACQUITY UPLC BEH C18 analytical column (50 mm × 2.1 mm, 1.7 μm) with 0.1% formic acid in water (mobile phase A) and acetonitrile with 0.1% formic acid (mobile phase B). A gradient at a flow rate of 0.50 mL/min was utilized, with a total run time of 2.0 min. Substrates were monitored using electrospray ionization (ESI) with multiple reaction monitoring (MRM) in the positive or negative ion mode.
(19) Intravenous dose at 5 mg/kg with male rats: CL = 10.9 L h^{-1} kg^{-1}; V_{ss} = 4.69 L/kg; $T_{1/2}$ = 0.37 h; AUC_{inf} = 0.11 μM·h.
(20) A high-throughput RLM assay as a surrogate of MLM allowed us to identify promising compounds for further PK and PD studies in mice.
(21) (a) Floby, E.; Briem, S.; Terelius, Y.; Sohlenius-Sternbeck, A.-K. The use of a cocktail of probe substrates for drug-metabolizing enzymes for the assessment of the metabolic capacity of hepatocyte preparations. *Xenobiotica* **2004**, *34*, 949−959. (b) Bissell, D. M.; Guzelian, P. S. Phenotypic stability of adult rat hepatocytes in primary monolayer culture. *Ann. N.Y. Acad. Sci.* **1980**, *249*, 85−98.
(22) For the first example of S···O═C interaction, see the following: Goldstein, B. M.; Mao, D. T.; Marquez, V. E. Ara-tiazofurin: conservation of structural features in an unusual thiazole nucleoside. *J. Med. Chem.* **1988**, *31*, 1026−1031.
(23) For more details, see the Supporting Information.
(24) Selected compounds **22** and **49** showed relatively low oral bioavailability at 13% and 21%, respectively, likely due to their moderate solubility. The oral bioavailability (% F) is based on 2 mg/kg po PK study in rats.
(25) Huang, L.; Chen, A.; Roberts, J.; Janosky, B.; Be, X.; Berry, L.; Lin, M.-H. J. Use of uptake intrinsic clearance from attached rat hepatocytes to predict hepatic clearance for poorly permeable compounds. *Xenobiotica* **2012**, *42* (9), 830−840.
(26) The PARP1 biochemical assay was purchased as a kit from Trevigen (catalog no. 4676-096-K) and used per manufacturer's recommendations. The PARP2 biochemical assay was purchased as a kit from BPS (catalog no. 80552) and used per manufacturer's recommendations. **22**: PARP1 IC_{50} = undefined, PARP2 IC_{50} = 2.45 μM. **49**: PARP1 IC_{50} = undefined, PARP2 IC_{50} = 1.76 μM.
(27) The kinase profiling was done using the KINOMEscan service provided by DiscoveRx (formerly Ambit Bioseciences).